# SUPPLEMENTAL INFORMATION

**Super- soft, firm, and strong elastomers toward replication of tissue viscoelastic response**

Erfan Dashtimoghadam,[1] Mitchell Maw,[1] Andrew N. Keith,[1] Foad Vashahi,[1] Verena Kempkes,[1]

Yulia D. Gordievskaya, Elena Yu. Kramarenko,[2] Abdelaziz Lallam,[3] Egor A. Bersenev,[2] Dimitri

A. Ivanov,[2,3,4] Yuan Tian,[1] Andrey V. Dobrynin,[1] Mohammad Vatankhah-Varnosfaderani,[1*]

Sergei S. Sheiko[1*]

[1]*Department of Chemistry, University of North Carolina at Chapel Hill, 27599, USA*

[2]*Lomonosov Moscow State University, Leninskie Gory 1, 119991, Moscow, Russian Federation*

[3]*Institut de Sciences des Matériaux de Mulhouse-IS2M, CNRS UMR 7361, 15, rue Jean Starcky,
F-68057 Mulhouse, France.*

[4]*Sirius University of Science and Technology, 1 Olympic Ave, 354340, Sochi, Russian Federation*

**Table of Contents**

**S1 Materials and Synthesis**

**S1.1 Materials.** Tetrahydrofuran (THF), toluene, acetone, hexane, acetonitrile, and p-xylene were purchased from Fisher Scientific and used as received. Styrene and n-butyl acrylate (BA) were purchased from Fisher Scientific and were passed twice through basic alumina column to remove inhibitor. 2,2'-Azobis(2-methylpropionitrile) (AIBN, 98%), Methyl 2-(dodecylthiocarbonothioylthio)-2-methylpropionate (CTA, 97%), α-bromoisobutyryl bromide (BiBB, 98%), 2-Hydroxyethyl 2-bromoisobutyrate (HEBIB, 95%), methacryloyl chloride (MACl, 97%), triethylamine (TEA), copper(I) bromide (CuBr, 99.999%), $tris$[2-(dimethylamino)ethyl]amine (Me$_6$TREN), N,N,N',N'',N''-Pentamethyldiethylenetriamine (PMDETA), dibutyltin dilaurate (DBTDL, 95%), 2-isocyanatoehtyl methacrylate (IEM, 98%), tetrabutylammonium bromide (TBAB, 98%), 33 wt. % hydrobromic acid solution in acetic acid (HBr), aluminum oxide (activated, basic, Brockmann I), silica gel (230-400 mesh) were purchased from Sigma Aldrich and used as received. Poly(ethylene glycol) methacrylate (PEGMA, $M_n$ = 500 g/mol) was obtained from Sigma Aldrich and purified by passing (twice) through basic alumina column to remove inhibitor. Monomethacryloxypropyl terminated polydimethylsiloxane (PDMSMA, MCR-M11, $M_n$ = 1000 g/mol) and potassium methacrylate (KOMA, 95-100%) were obtained from Gelest. The former was purified using a basic alumina column to remove inhibitor and the latter was used as received. RB HR-PIB-1000 was obtained from RB Products and used as received. Methyl methacrylate (MMA, 99%) and styrene (Sty, 99%) was obtained from Fisher Scientific and purified using a basic alumina column to remove inhibitor. Teflon petri dishes were purchased from Welch Flourocarbon.

**CRP OF poly[MMA-*g*-(PDMS/PMMA)] AND poly[nBA-*ran*-MMA-*g*-(PDMS/PMMA)]**

**S1.2 Functionalization of PEGMA-OH.** PEGMA (40g, 40mmol), TEA (4.04g, 40mmol), THF (40mL) and a stir bar were added to a round bottom flask and left to stir at 0°C for 30 minutes. BiBB (9.16g, 4.92mL, 40mmol) was added dropwise over 15 minutes to the reaction mixture. The solution was brought to room temperature and left to stir for an additional 2 hours. The mixture was centrifuged and the organic layer decanted and concentrated under vacuum. The reaction mixture was then passed through a silica column and dried overnight resulting in a functionalized PEGMA-Br ATRP initiator as a functional site for future polymerization.

**S1.3 Grafting Through RAFT copolymerization.** For a graft copolymer macroinitiator with architectural parameters of $n_g = 8$, $n_{sc} = 14$, $n_x = 100$, PDMSMA (20g, 20mmol), BA (17.9g, 0.14mol), PEGMA-Br (1.04g, 1.6mmol), CTA (21.8µL, 57.6µmol), AIBN (2.3mg, 14.4µmol), toluene (20mL), and a stir bar were added to a Schlenk flask. The solution was bubbled with dry nitrogen for 1 hour, then submerged into an oil bath at 70°C, and left to polymerize overnight. The polymerization was quenched by opening the flask, the reaction mixture dried, and the conversion determined by ^{1}H-NMR to be 88% of a random PDMSMA, PEGMA-Br and PBA copolymer with $n_{bb} = 1935$ (Fig. S5). The polymer mixture was precipitated from methanol 2-3 times to remove residual PDMSMA and dried under vacuum until a constant mass was reached (Fig. S6).

**S1.4 Grafting From to synthesize poly[MMA-*g*-(PDMS/PMMA)] via ATRP.** The resulting polymer brushes polymerized by RAFT were then used as macroinitiators for ATRP growth of linear MMA. For a typical graft copolymer plastomer, graft copolymer initiator (2g), excess MMA (2g), M₆TREN (5uL, 18.7µmol), toluene (50mL) and a stir bar were added to a Schlenk flask. The solution was bubbled with dry nitrogen for 1 hr then Cu(I)Br (2.8 mg, 18.7µmol) was quickly added to the reaction mixture under nitrogen atmosphere. The flask was sealed, purged for an additional 15 minutes, and then immersed in an oil bath at 45°C. The polymerization was visually monitored to avoid gelation of the growing chains. The polymerization was quenched at various times to afford to afford a series of graft copolymers with increasing PMMA ratio. Note, reaction times were relatively short (0.5-1.5hr) using 20mL of toluene before observed gelation similarly documented in the literature,[1] however excess toluene (>80mL) allowed for larger growth time (2hr) of PMMA chains before gelation. All resulting graft copolymer plastomers were swelled and washed two-three times with acetone to remove PMMA homopolymer, and then swelled and washed two-three times with hexanes to remove unreacted brushes. These impurities typically represent <10% of the total yield.[2] Finally, the $n_A$ and $\phi_A$ of the PMMA side chains were measured by ^{1}H-NMR (Fig. S8-S12) as summarized in Table 1, PEG appendage excluded. Samples were then dissolved in THF (75 wt% solvent) and poured into Teflon petri-dishes and left to dry overnight to yield films for further mechanical testing. Note that the grafting from approached exhibited synthetic limitations where $\phi_A$ did not exceed 0.07 due to insolubility between the growing A-g-B brush strand in residual monomer/solvent solution. Another factor may be the polarity/functionality of the RAFT end groups during ATRP. Further experimentation is needed to greater understand the interplay between attainable $\phi_A$ and $\chi$ of monomers and synthesized

polymer. Note: higher $\phi_A$ was attained by increasing $n_g$ in poly[nBA-*ran*-MMA-*g*-(PDMS/PMMA)] brush copolymers.



**Scheme 1.** A-g-B brush graft copolymer synthesis by CRP methods. Note: omitted RAFT end groups correspond with methyl 2-(dodecylthiocarbonothioylthio)-2-methylpropionate, CTA. (at brackets)

## FREE-RADICAL POLYMERIZATION OF poly[nBA-*ran*-MMA-*g*-(PDMS/PS)] and poly[nBA-*ran*-MMA-*g*-(PIB/PS)]]

[(PMMA)-g-(PDMS)] and [(PMMA)-g-(PDMS)-PBA] brush graft copolymers synthesized by CRP, shown in Fig. 2 and 3, are inefficient temporally and require comprehensive purification of substantial quantities of metal-ligand complex.[3,4] For more efficient polymerization, A-g-B brush graft copolymers can also be polymerized by UV initiated free-radical (FR) polymerization, though at a detriment to precise determination of $n_{bb}$ (Đ~2). Turning to free-radical polymerization of A-g-B brush copolymers, both brush side chain and A-block chain must be pre-synthesized into side chain macromonomers (S1.5-1.8) and subsequently grafted through (S1.9). Grafting through the oligomeric reagents introduces other synthetic consideration including interaction energy between side-chain macromonomers, A-block macromonomers, and solubility.

**S1.5 Anti-Markovnikov bromination of HR-PIB 1000, $n_{sc} = 18$.** To a 250 mL round bottom flask equipped with a stir bar, 50g (0.05mmol) RB HR-PIB ($M_n = 1000$ g/mol, Đ ~ 1.9) and hexane (150mL) was added and placed in an ice bath. The solution was bubbled with oxygen for 30 minutes at 0°C and 24.3g of 33 w/w% HBr (0.1mol) in EtOAc was added dropwise to the flask with vigorous stirring. The reaction stirred for 2 hrs at 0°C and brought up to room temperature where it was left to stir overnight. Stirring was ceased and the resultant anti-Markovnikov bromine functionalized PIB oligomer was washed with $H_2O/Na_2CO_3$ twice, dried with anhydrous $MgSO_4$, and passed through a short $SiO_2$ column. The hexanes were evaporated by bubbling with air

yielding 98% functionalized polymer (determined by $^1$H-NMR, Fig. S15). No residual olefin residue was present suggesting higher conversion.

**S1.6 Synthesis of PIB macromonomer, $n_{sc} = 18$.** The functionalized oligomer (45g, 0.042mol) was dissolved in THF (350mL) and transferred to an oven dried 500mL round bottom flask equipped with a stir bar. The solution was charged with 26.0g KOMA (0.21mol) and 67.6g TBAB (0.25mol) and stirred for 36 hrs at 45°C. The solution was centrifuged to remove residual salt and unreacted reagent. Subsequently, the solution was condensed by bubbling with air and washed with H$_2$O/hexane twice. The organic layer was separated, dried with anhydrous MgSO$_4$, and ran through a SiO$_2$ column twice yielding PIB ($n_{sc} = 18$) macromonomer product (99% conversion, ~90% yield). Again, no residual peaks were present from the α-hydrogens suggesting higher yield. $^1$H-NMR of the synthetic progression is shown in Fig. S15.



**Scheme 2.** PIB macromonomer synthesis.

**S1.7 Synthesis of PS oligomers.** ATRP of polystyrene homopolymer was performed with a target $n_A = 60$ at 34% conversion to avoid large viscosities at higher conversion. Styrene (100g, 0.96mol), HEBIB (1.16g, 5.5mmol), PMDETA (0.095g, 0.114mL, 0.55mmol), and a stir bar were added to a Schlenk flask. The solution was bubbled with dry nitrogen for 1 hour then Cu(I)Br (0.079g, 0.55mmol) was quickly added to the reaction mixture under nitrogen atmosphere. The flask was sealed, purged for an additional 15 minutes, and then immersed in an oil bath at 90°C. The reaction mixture was left to polymerize for 14 hrs to receive a 34% conversion ($n_{sc} = 60$) and the reaction was quenched by exposing the mixture to oxygen (Fig. S14). The mixture was centrifuged and gravity filtered to remove residual Cu-ligand complex. Residual styrene monomer was evaporated and the remaining PS oligomer was dissolved in minimal THF and crashed in excess methanol (1:10, THF:Methanol by volume) 3 times. The washed PS oligomer was dried overnight at room temperature under reduced pressure to remove any residual solvent.

**S1.8 Synthesis of PS (DP = 60) macromonomer.** The PS oligomer (30 g, 4.8mmol, DP = 60) was transferred to a round bottom flask sealed by rubber septum and parafilm and dissolved in 60 ml of THF. Once the PS was fully dissolved, 0.05g (47μL, 80μmol) dibutyltin dilaurate was added to the solution, it was subsequently purged of oxygen by bubbling the solution with nitrogen for 10 minutes. IEM (0.82g, 0.75mL, 5.3mmol) was added dropwise to the round bottom flask under constant stirring. Nitrogen was removed from the flask, and the solution was set to stir for 18hr. The subsequent solution was further diluted with THF (5-10x) and passed through silica column twice. The purified mixture was dried under reduced pressure and characterized by $^1$H-NMR (Fig. S14). H$^1$-NMR reveals 80% conversion so subsequent calculations for $\phi_A$ for performed considering an 80% ratio of macromonomers.
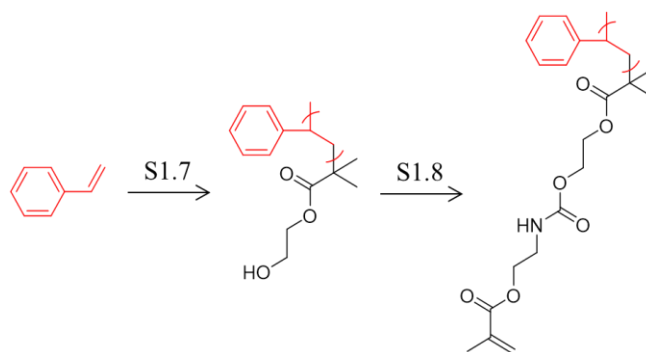


**Scheme 3.** PS macromonomer synthesis.

**S1.9 FR polymerization of A-g-B brush copolymers by grafting through**. A Schlenk flask was charged with appropriate molar quantities of side-chain macromonomer (PDMS, PIB), spacer (n-BA), A-block macromonomer (PS), 1:1 volume of p-xylene, and 0.15 mol% initiator (BAPO). The flask was shielded from light and purged with nitrogen for 30 minutes. Subsequently, the solution was removed from nitrogen and allowed to polymerize under UV-light for 18hr. The solution exhibits a light-yellow color upon introduction to the UV-light but returns to transparent after polymerization. The unwashed polymer solution was caste in a Teflon mold at 60°C and dried overnight. The resultant polymer was washed according to chemistry. poly[nBA-*ran*-MMA-*g*-(PIB/PS)]: the unwashed polymer was dissolved in THF and crashed with acetonitrile (1:1.2, THF:acetonitrile) 3 times (Fig. S1). The washed polymer was dissolved in p-xylene once more and caste into a Teflon petri-dishes (Welch Fluorocarbon) at 60°C and dried overnight to be characterized by $^1$H-NMR where no macromonomer peaks remained (Fig. S16). poly[nBA-*ran*-MMA-*g*-(PDMS/PS)]: the unwashed polymer was dissolved in acetone and crashed out in acetonitrile (2:1, acetone:acetonitrile). This wash was repeated three times. The washed polymer

was dissolved in p-xylene once more and caste into a Teflon petri-dishes and dried overnight to be characterized by $^1$H-NMR where no macromonomer peaks remained. Note that unreacted reagents act as diluent and decrease the modulus of the network. Comparing washed and unwashed A-g-B network stress-strain curves exhibit this behavior (Fig. S24). The number average molecular weight ($M_n$) of the A-g-B brush polymer stand was determined by light scattering detection during gel-permeation chromatography (Fig. S18, S20)

Ex. synthetic calculations. poly[nBA-*ran*-MMA-*g*-(PIB/PS)]. Sample: 030722_1. 2.00g n-butyl acrylate (15.6mmol), 2.41g PIB macromonomer (2.23mmol), 0.27g PS macromonomer (43µmol, 80% conversion PS mixture, total mass 0.34g), 7mg BAPO (17µmol, 0.15w/w%), and 4.5mL of p-xylene.
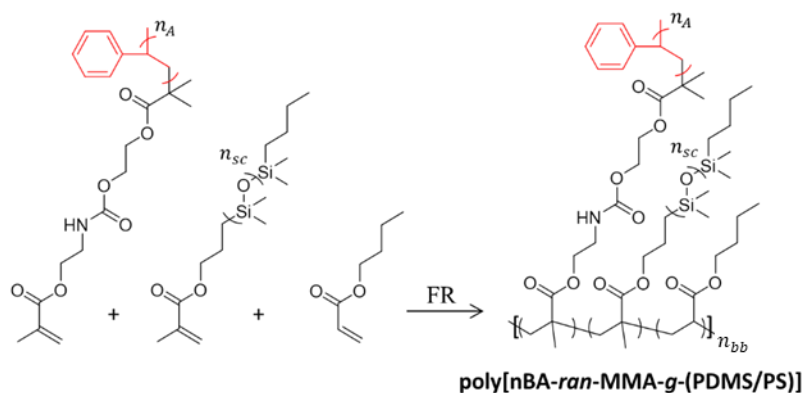


**Scheme 4.** Polymerization of poly[nBA-*ran*-MMA-*g*-(PDMS/PS)] brush graft copolymers.
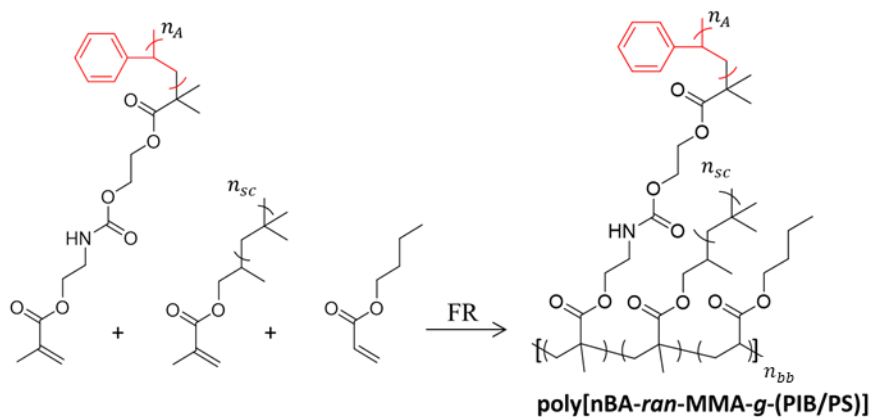


**Scheme 5.** Polymerization of poly[nBA-*ran*-MMA-*g*-(PIB/PS)] brush graft copolymers.

Wash – 1.2:1, Acetonitrile:THF

Linear PBA          PS Macromonomer     [1265, 503, 18, 8, 60, 0.048]
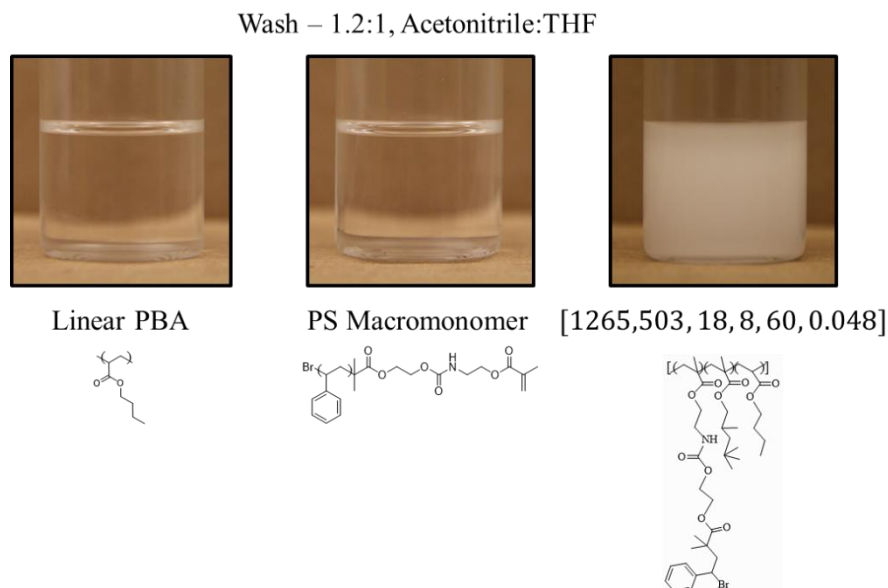
**Fig. S1**. Example purification of A-g-B brush copolymers, poly[nBA-*ran*-MMA-*g*-(PIB/PS)].

## S2 Materials Characterization

**S2.1 Atomic force microscopy.** Monolayers of A-g-B brush copolymers were prepared by Langmuir-Blodget using a KSV 5000 onto a muscovite sheet (Fig. 2a,b). The monolayer was formed by diluting the polymer in dichloromethane to 0.3 mg/mL and dispersing 75 µL onto the water reservoir. The muscovite sheet was removed from the water reservoir at a 5mm/min once the surface tension had reached 0.5 mN/m, forming a polymer monolayer on the muscovite sheet. Obtaining an image with clustered domains was achieved by forming a less dense layer of polymers on the surface of the water with a surface tension ~0.4 mN/m. Imaging was performed in PeakForce QNM mode using a multimode AFM (Brüker) with a nanoscope V controller and silicon nitride (Scanasyst-Air by Brüker, resonance frequency of 50-90 HZ and spring constant of 0.4 N/m). Inter-brush distance was calculated by the mean of 50 individual measurements between brush peaks on the AFM height micrograph on the Nanoscope Analysis software (Brüker).

**S2.2 Small angle X-ray scattering (SAXS).** SAXS measurements were performed on the ID02 and BM26 beamlines of the ESRF (grenoble, France). The experiments at ID02 were conducted in transmittance geometry with a photon energy of 12.46 KeV. The total phototon flux on the sample is estimated to $9.1^{11}$ photons persecond with the monochromatic incident X-ray beam collimated to a footprint of 100 x 200 µm$^2$ (V x H) allowing an acquisition time of less than 100 ms per frame. The $q$ values ($q = 4\pi \sin(\theta) / \lambda$ range from $7.5 \times 10^{-3}$ nm$^{-1}$ to 3 nm$^{-1}$ at a sample

detector distance of 2 m. Optimization of the signal-noise ratio through a Rayonix MX-170HS in a 35 m long vacuum flight tube was achieved through the binning of 2x2 pixel leading to an effective pixel size of 89 μm in both directions.

SAXS images at BM26 were collected using a Pilatus 1M detector (169 mm x 179 mm active area). The experiments were performed in transmission geometry using a photon energy of 12.99 keV and sample-to-detector distance of 2.8 m. Mechanical stretching of the samples was carried out using tensile cell from Linkam (LINKAM TST 350). The data correction, calibration, and integration was performed using the fast azimuthal integration Python library. (reference to insert : G. Ashiotis, A. Deschildre, Z. Nawaz, J. P. Wright, D. Karkoulis, F. E. Picca and J. Kieffer Journal of Applied Crystallography, 2015, 48, 510-519). To compute form factor parameters 1D SAXS curves were fit to a scattering for a polydisperse population of spheres with uniform scattering length density. The distribution of radii is a Gaussian distribution. The data modelling and analysis were performed using the SANS & USANS data reduction and analysis package provided by NIST[5] for Igor Pro 6.7.3.2 environment from WaveMetrics Ltd.

**S2.3 Uniaxial tensile stress strain measurements.** Dog bone shaped samples with bridge dimensions of 12 mm × 2 mm × 1 mm were loaded into an RSA-G2 DMA (TA Instruments) and subjected to uniaxial extension at 20˚C and constant strain rate of $0.005$ s$^{-1}$ for PDMS samples and $0.001$ s$^{-1}$ for PIB samples. Samples were stretched until rupture, revealing the entire mechanical profile. In each case, mechanical tests were conducted in triplicate to ensure accuracy of the data. The elongation ratio $\lambda$ for uniaxial network deformation is defined as the ratio of the sample's instantaneous size $L$ to its initial size $L_0$, $\lambda = L/L_0$. At small and intermediate deformation range, all stress-deformation curves, $\sigma_{true}(\lambda)$, follow non-linear equation of network elasticity [6] and switch to a linear scaling, $\sigma_{true}(\lambda) \sim \lambda$, at large deformations (see Fig. S2).[1,7] Network elastic parameters $(E, E_0, \beta)$ obtained from the fitting of stress-deformation curves were averaged over sample triplicates, while reported $\lambda_{max}$ and $\sigma_{max}$ are given for the largest of each triplicate.

**Fitting structural modulus ($E$) and strain stiffening ($\beta$).** In the elastic deformation regime, raw stress strain curves for uniaxial deformation were fitted to the following non-linear equation [6]

$$\sigma_{true}(\lambda) = \frac{E}{9}(\lambda^2 - \lambda^{-1})\left(1 + 2\left(1 - \frac{\beta(\lambda^2 + 2\lambda^{-1})}{3}\right)^{-2}\right). \tag{S1}$$

with $E$ and $\beta$ being fitting parameters as illustrated in Fig. S2. The corresponding Young's modulus, $E_0$, at small deformations, $\lambda \to 1$, is given by

$$E_0 = \frac{E}{3}(1 + 2(1 - \beta)^{-2}). \tag{S2}$$



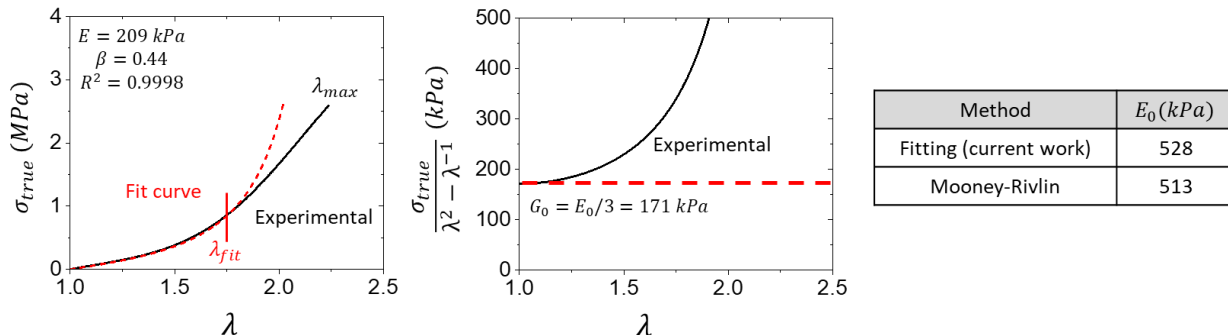| Method | $E_0 (kPa)$ |
|---|---|
| Fitting (current work) | 528 |
| Mooney-Rivlin | 513 |

**Fig. S2.** Comparing fitting vs. Mooney-Rivlin method for determination of $E_0$. The fitting method shows good agreement with the Mooney-Rivlin method within 3 percent variation. [(528kPa - 513kPa)/(513kPa)] * 100 = 2.9%. $\dot{\varepsilon}$ =0.005, T=22°C.

**S2.4 Rheology.** Frequency and temperature sweeps were performed on the ARES-G2 Rheomoeter (TA instruments) with 8mm compression plate geometries. Samples were prepared by cutting 8mm diameter disks with approximate hieght of 1mm (exact height was specified in the rheometer for each sample). The frequency sweep was performed from 0.01 to 100 Hz (within the viscoelastic PSA range) at 22°C at with $\varepsilon = 0.05$ to ensure adequate contact area between the compression plate and sample. The temperature sweep was performed from 20°C to 200°C with $\varepsilon = 0.05$ oscillating at 1 Hz. Noisy data in melt state at high temperatures as a consequence to the infacial contact area between the compression plate and sample decreasing were removed.

**S2.5 Fused-filament fabrication 3D printing.** Fused-filament fabrication 3D printing was performed with poly[nBA-*ran*-MMA-*g*-(PIB/PS)] sample 030722_2 using a Cellink BioX 3D printer where shape stl. files were created with Tinkercad (for dogbones) and Photoshop (for UNC logo) (Fig. 4c). The polymer resevoir was heated to 150°C to ensure adhequate flow and extuded at a pressure of 120 kPa. Multiple dog-bone shape samples were printed with one left raw and the other annealed at 100°C for 5 minutes (Fig. S31).

**S2.6 Modified probe tack tesiting.** The $W_{adh}$ was measured using a modified version of the probe tack test using a G2-RSA DMA.[8] The top arm contained a 2 mm diameter probe and the bottom

arm was a 25 mm plate both with roughness of 0.5 microns (TA instruments). Segments of sample were placed on the bottom compression plate and allowed to wet the surface over time. In addition, a rubber roller was used to apply light pressure ensuring the adhesive bond between the elastomer and bottom plate (acting as carrier) remained intact during measurement.
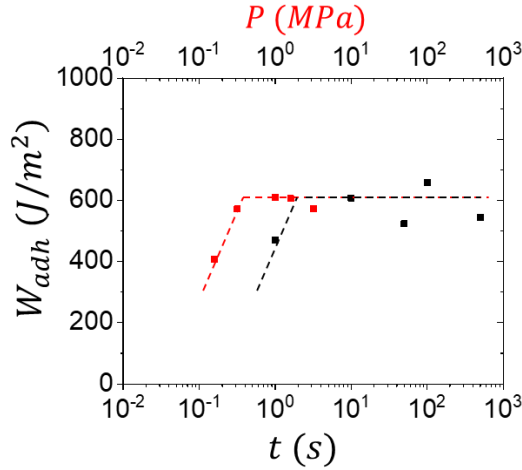


**Fig. S3**. Optimization of contact pressure and dwelling time. The modified probe tack test was performed using a control PSA elastomer independently changing the contact pressure ($P$) and contact time ($t$) in effort to maximize the contact area of the PSA bond. The degree of contact area coverage and subsequent $W_{adh}$, calculated as

$$W_{adh} = h_o \int_0^{\varepsilon_{max}} \sigma_{eng}(\varepsilon)d\varepsilon \ , \tag{S3}$$

where $h_0$ is the initial thickness of the adhesive film and $\varepsilon_{max}$ is the maximum strain before catastrophic failure of the bond, plateaued ~ 600 J/m². Parameters of 1 MPa contact pressure and 100s contact time were used for further experimentation.

Each run consisted of compression at 0.01 mm/s until a contact pressure, $P = 1 \, MPa$, was attained. The probe was held at a dwell time, $t = 100 \, s$ and removed at 1mm/s for debonding.
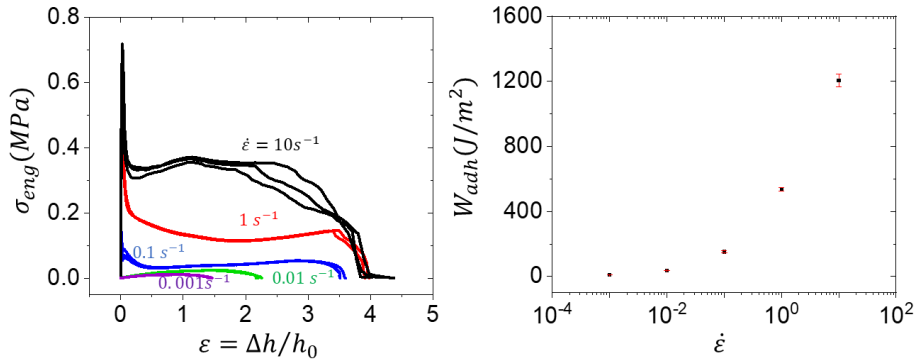


**Fig. S4.** Repeatability of modified probe tack test experiment. The modified probe tack was performed 3 times at the various debonding rates on a control brush PSA. The experimental procedure yeilds less than 4 percent deviation in $W_{adh}$ between tests at the same strain rate. $h_0 \sim$1mm, T=22°C.

**S2.7. Gel-permeation chromatography (GPC).** The molecular weight of the A-g-B brush copolymers synthesized by grafting through free-radical polymerization was determined by GPC using a Tosoh EcoSEC *Elite* GPC system eqiped with a TSKgel Super HM-M (17392) column maintained at 40°C with an RI detector and Tosoh LENS[TM] 3 multiangle light scattering detector. Tetraydrofuran was used as themobile phase at a flow rate of 0.5 mL/min. Molecular weight and and dispersity is reported based on polystyrene standards. Note that molecular weight readings are not very reliable from the RI detection,[9] so molecular weights were reported from light scattering detection.
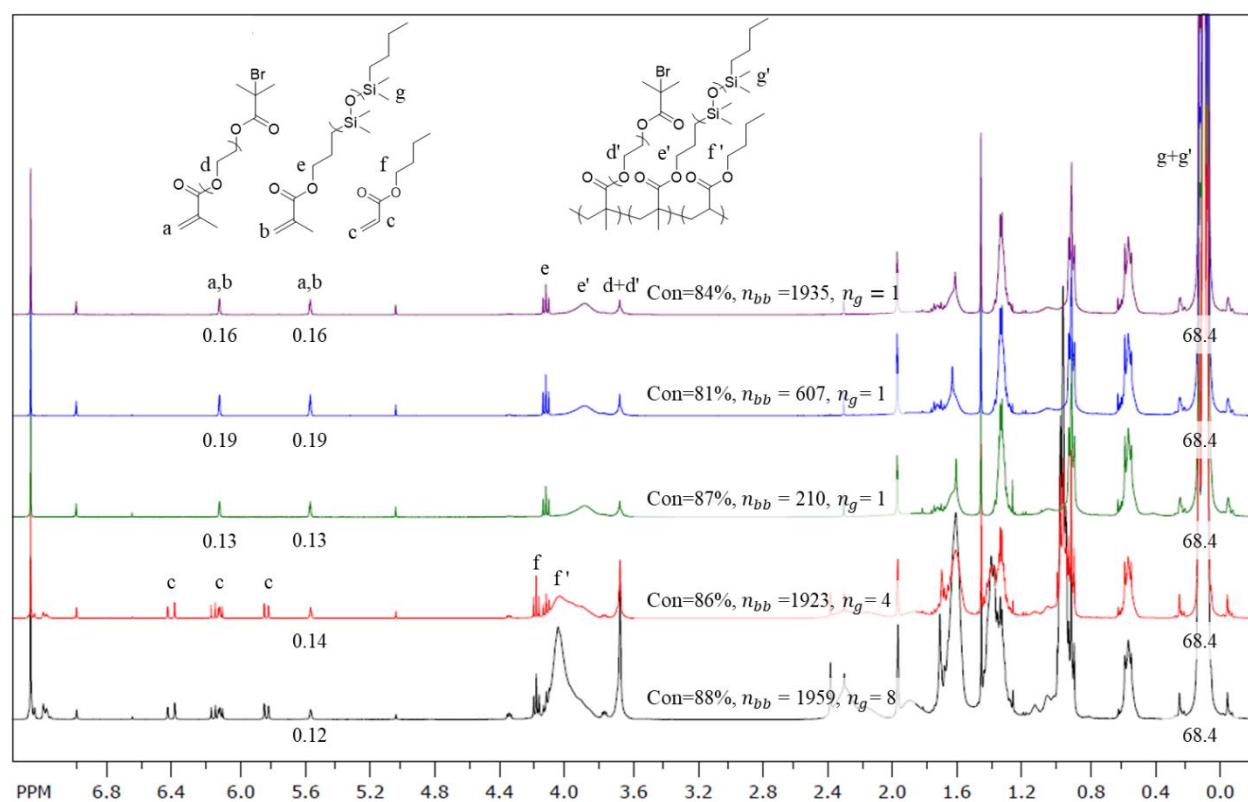


**Fig. S5.** ^{1}H-NMR of graft copolymer macroinitiators synthesized by CRP after termination (400 MHz, CDCl$_3$): 6.42, 6.14, 5.84 (C**H$_2$**=C**H**-C-, Residual BA monomer, d, 1H; m, 1H; d, 1H), 6.12, 5.56 (C**H$_2$**=C(CH$_3$)-C-, PDMS macromonomer, s, 1H), 4.18 ((C=O)-O-C**H$_2$**-, Residual BA monomer, t, 2H), 4.13 ((C=O)-O-C**H$_2$**-, PDMS macromonomer, t, 2H), 4.05 ((C=O)-O-C**H$_2$**-, PBA brush, m, 2H), 3.89 ((C=O)-O-C**H$_2$**-, PDMS brush, m, 2H), 3.67 (-O-C**H$_2$**-C**H$_2$**-, PEG side chain, m, 4H), 0.09 (-(Si(C**H$_3$**)$_2$-O)$_n$-, PDMS macromonomer and brush mixture, s, 68.4H). Conv. = [area(g+g')/68.4-area(a,b)/1]/[area(g+g')/68.4], $n_{bb}$ = Conv.*([PDMS]+[BA]+[PEGMA])/[I].
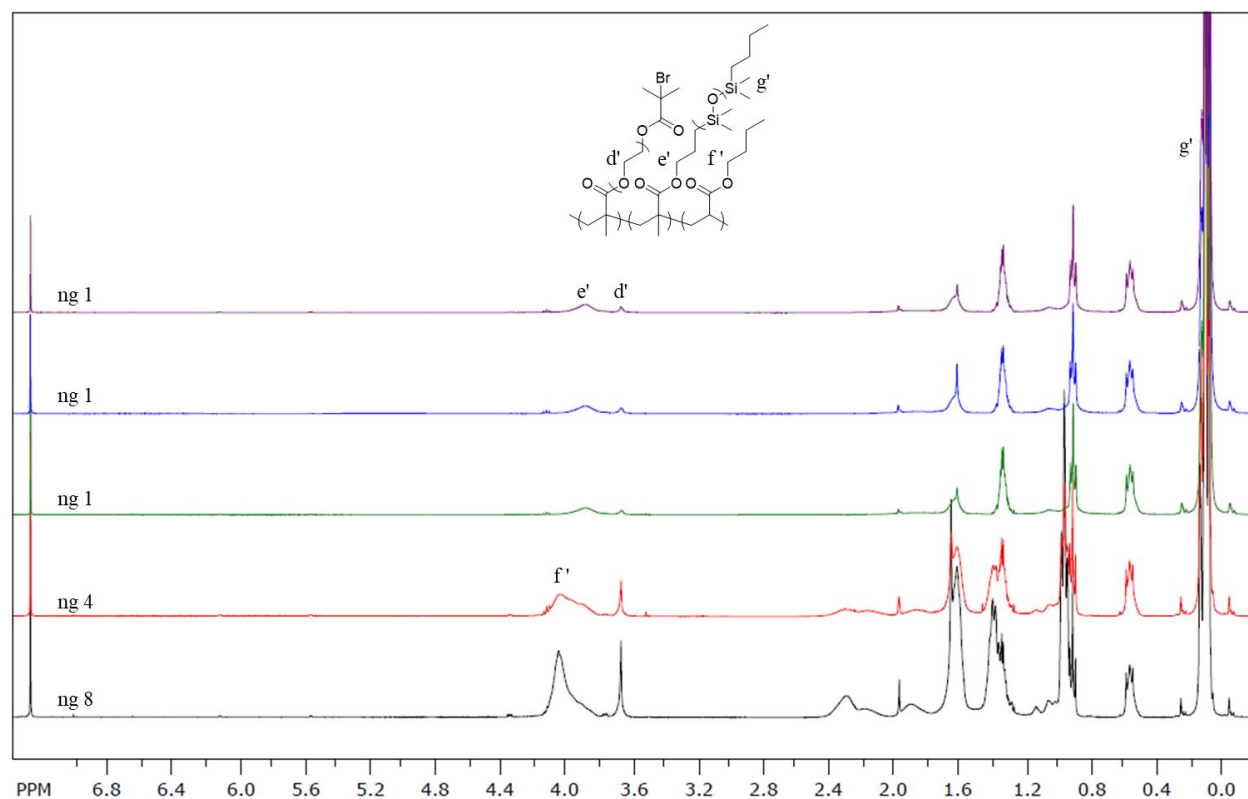
**Fig. S6.** $^1$H-NMR of purified graft copolymer macroinitiators synthesized by CRP (400 MHz, CDCl$_3$): 4.05 ((C=O)-O-**CH$_2$**-, PBA brush, m, 2H), 3.89 ((C=O)-O-**CH$_2$**-, PDMS brush, m, 2H), 3.67 (-O-**CH$_2$**-**CH$_2$**-, PEG side chain, m, 4H), 0.09 (-(Si(**CH$_3$**)$_2$-O)$_n$-, PDMS macromonomer and brush mixture, s, 68.4H). d'=0.295 for $n_g = 1$ backbones. d'=0.905 for $n_g = 4$ backbones. d'=1.951 for $n_g = 8$ backbones.
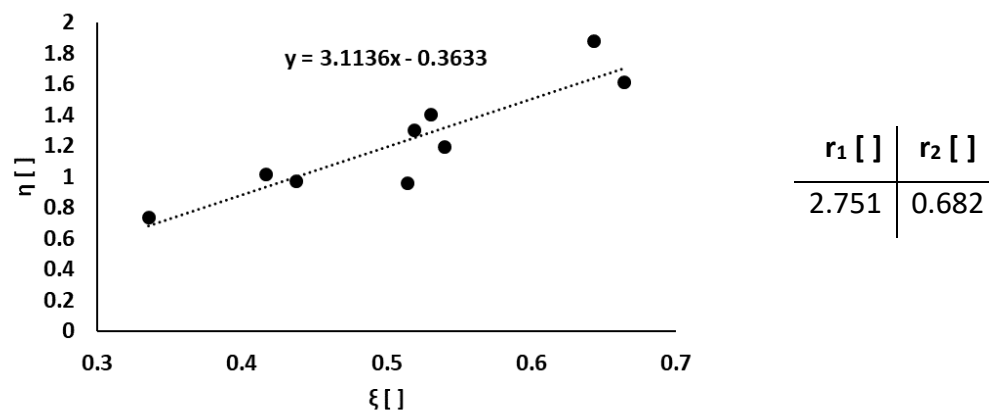


**Fig. S7.** Kelen-Tüdös plot for PDMS and PEGOH macromonomers during ATRP at 45°C. Reactivity ratios determined using the Kelen-Tüdös method[10] reveal gradient distribution of PDMSMA ($r_1$) and PEGMA ($r_2$) into a brush backbone. From this CRP method, we expect gradient distribution for RAFT used in this study us well due to differences in size and chemistry.
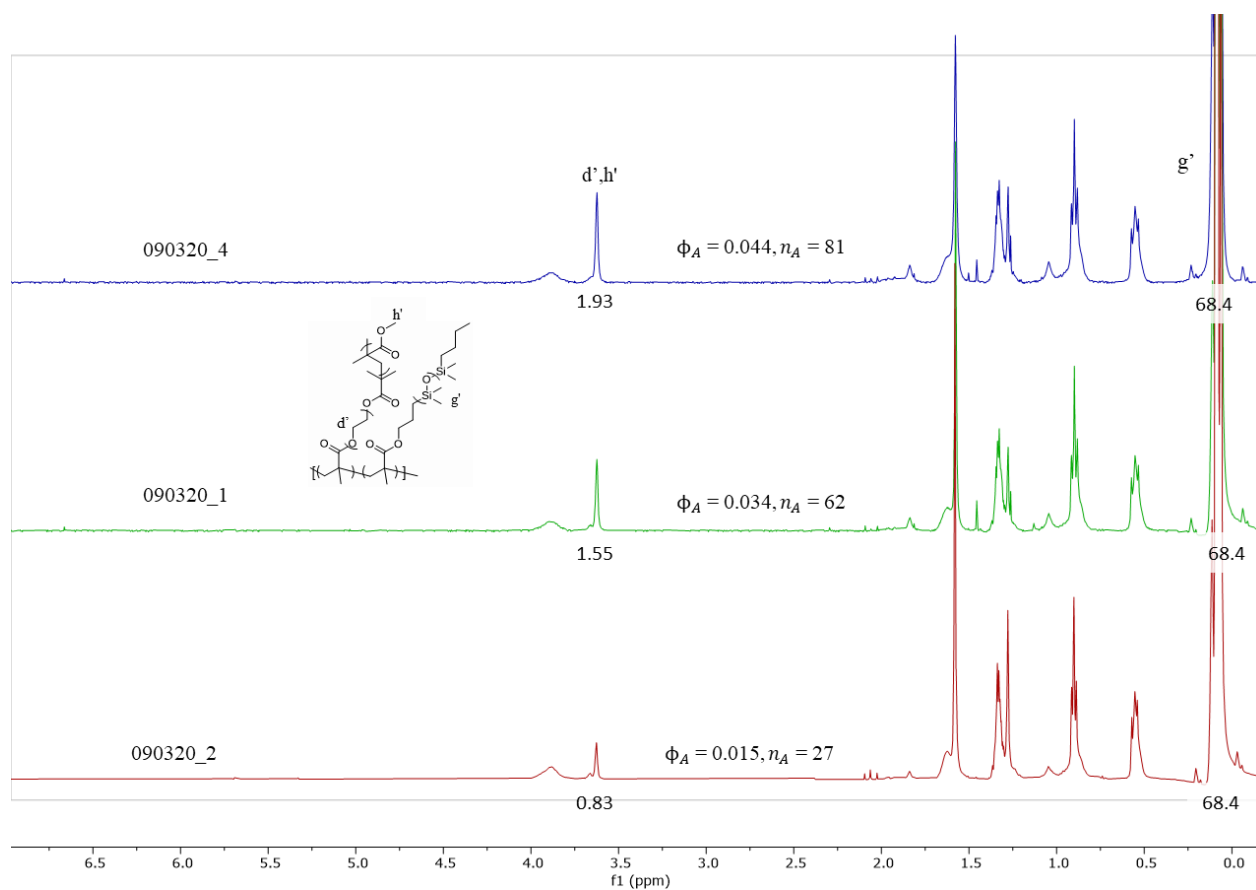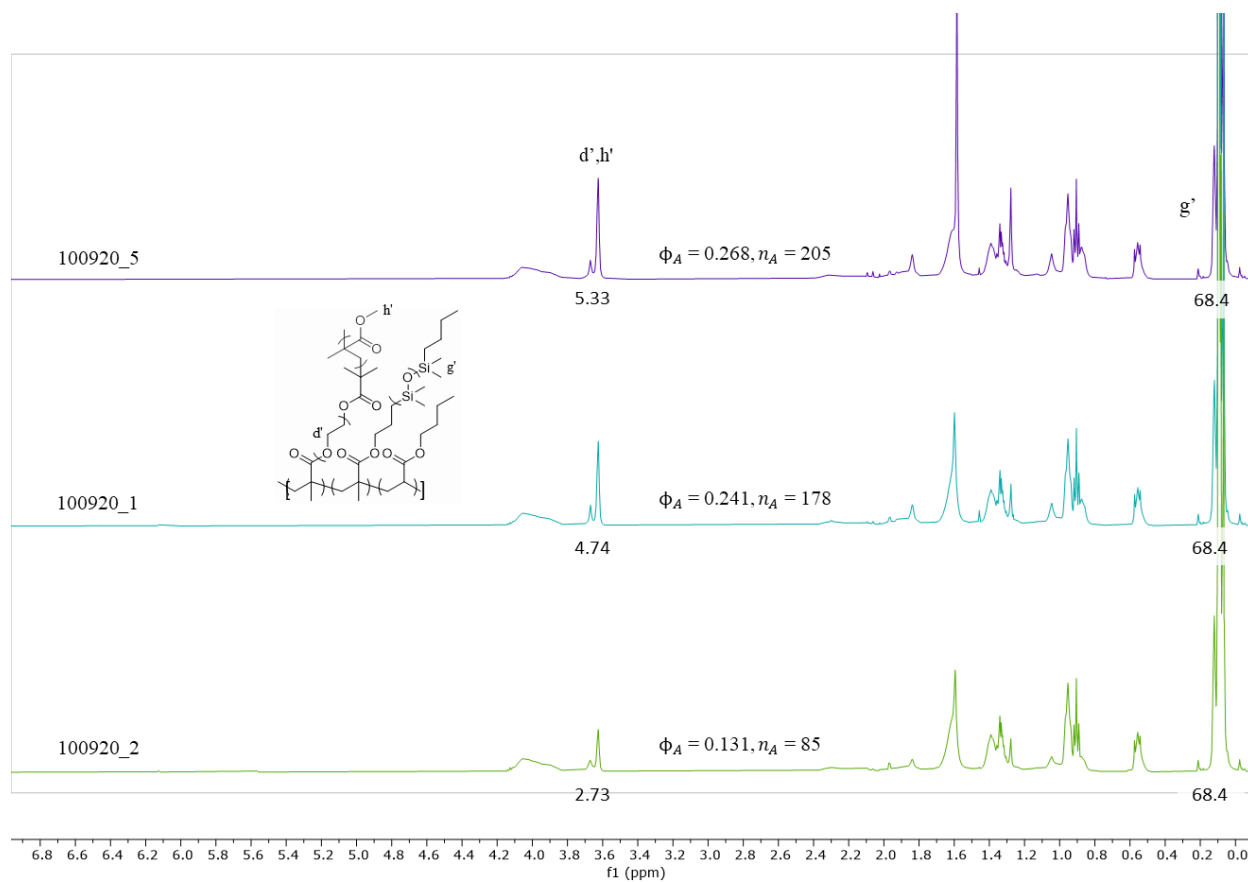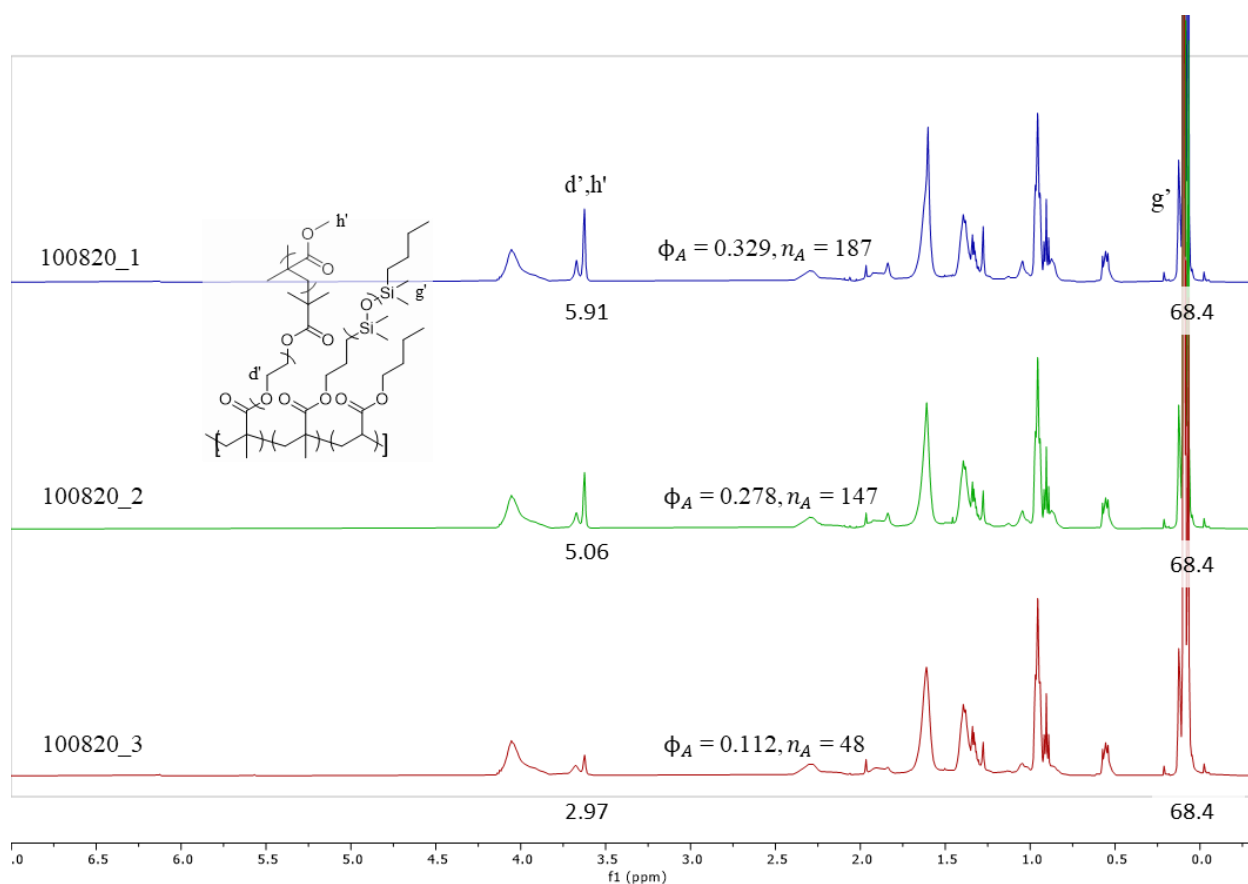
**Fig. S8.** $^1$H-NMR of purified poly[MMA-*g*-(PDMS/PMMA)] brush copolymer series $n_{bb}$=1935, $n_g$=1 synthesized by CRP (400 MHz, CDCl$_3$): 3.89 ((C=O)-O-C**H₂**-, PDMS brush, m, 2H), 3.62 ((C=O)-O-C**H₃**- and -O-C**H₂**-C**H₂**-, PMMA and PEG respectively, m, 7H), 0.09 (-(Si(C**H₃**)$_2$-O)$_n$, PDMS macromonomer and brush mixture, s, 68.4H).
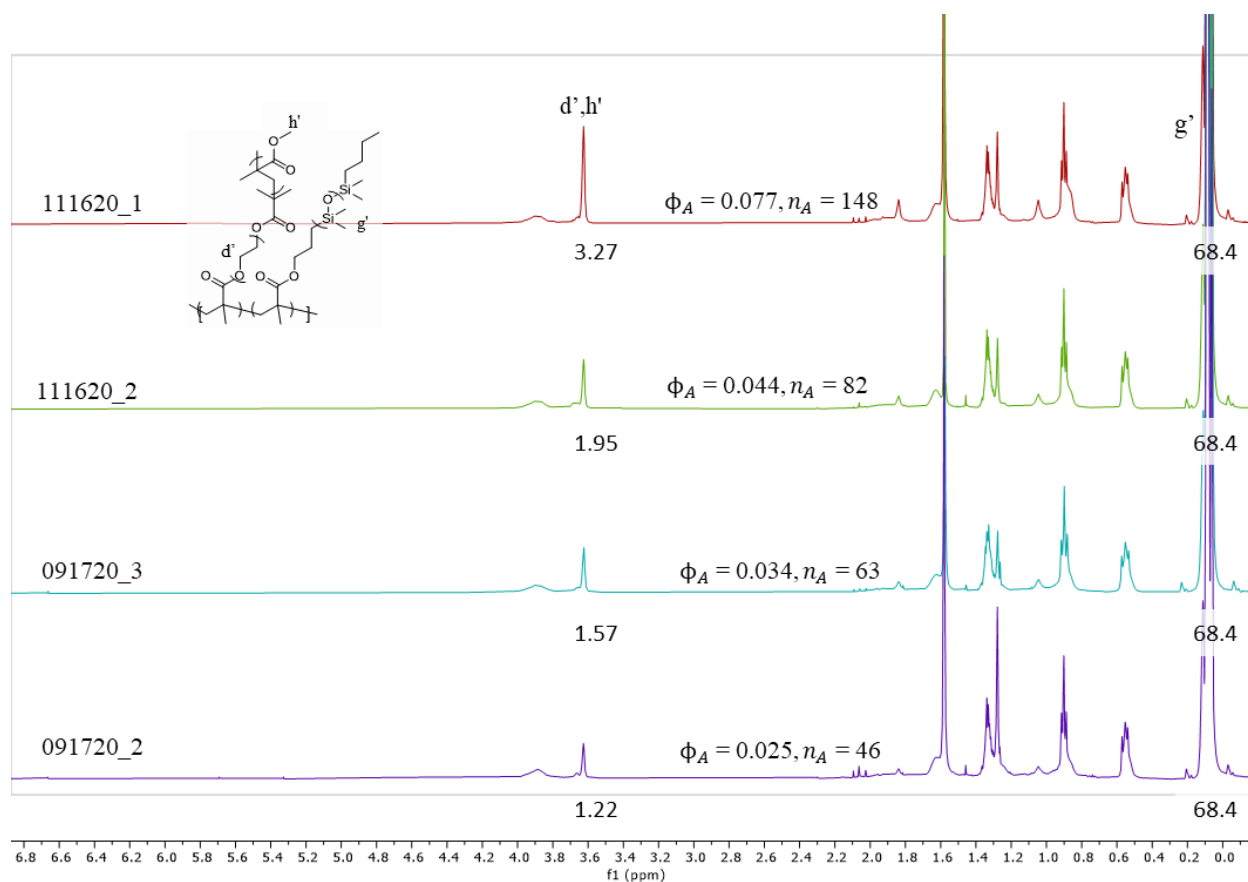
**Fig. S9.** $^1$H-NMR of purified poly[MMA-$g$-(PDMS/PMMA)] brush copolymer series $n_{bb}$=607, $n_g$=1 synthesized by CRP (400 MHz, CDCl$_3$): 3.89 ((C=O)-O-C**H$_2$**-, PDMS brush, m, 2H), 3.62 ((C=O)-O-C**H$_3$**- and -O-C**H$_2$**-C**H$_2$**-, PMMA and PEG respectively, m, 7H), 0.09 (-(Si(C**H$_3$**)$_2$-O)$_n$-, PDMS macromonomer and brush mixture, s, 68.4H).
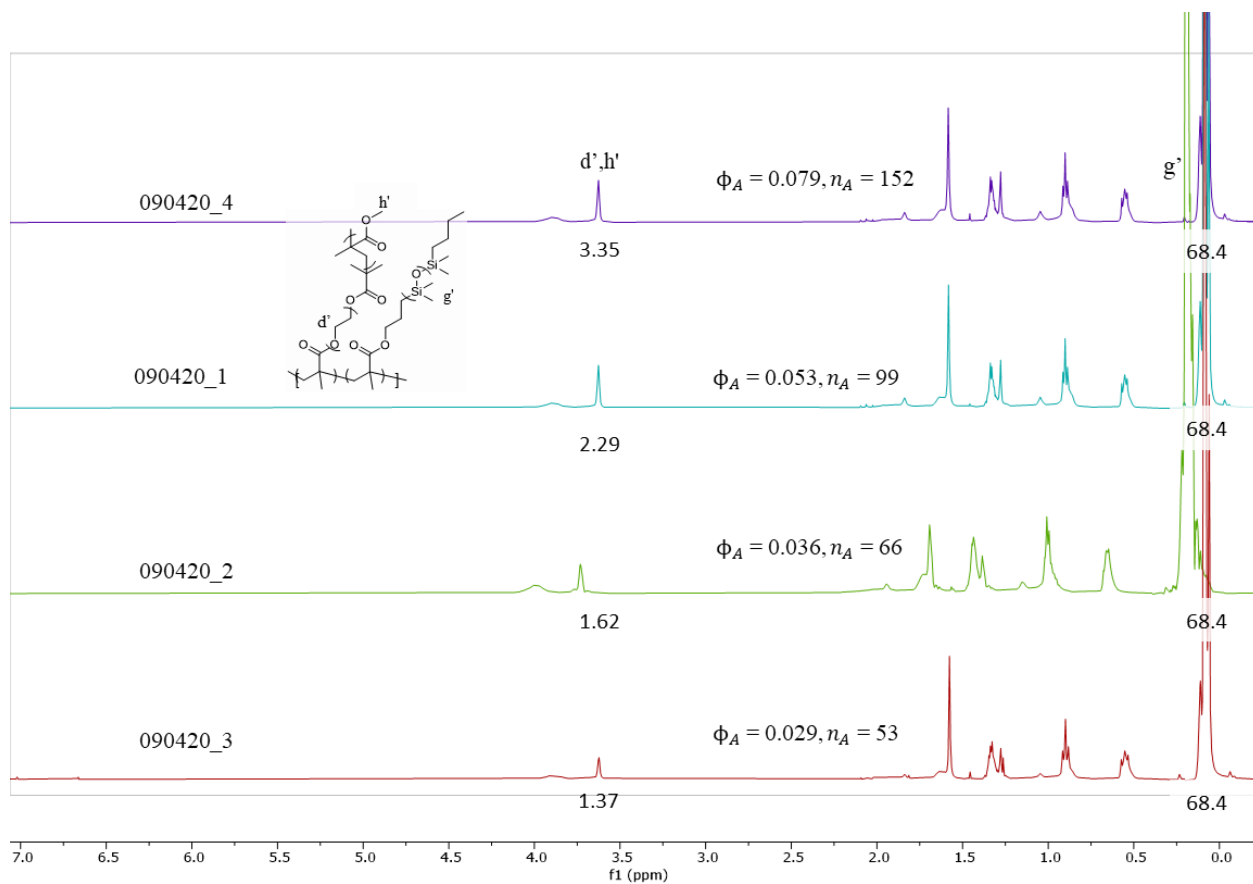
**Fig. S10.** $^1$H-NMR of purified poly[MMA-$g$-(PDMS/PMMA)] brush copolymer series $n_{bb}$=210, $n_g$=1 synthesized by CRP (400 MHz, CDCl$_3$): 3.89 ((C=O)-O-C**H$_2$**-, PDMS brush, m, 2H), 3.62 ((C=O)-O-C**H$_3$**- and -O-C**H$_2$**-C**H$_2$**-, PMMA and PEG respectively, m, 7H), 0.09 (-(Si(C**H$_3$**)$_2$-O)$_n$-, PDMS macromonomer and brush mixture, s, 68.4H).

Ex. calculation for densely grafted A-g-B networks. Sample 090320_4:

$$n_A = n_x \left( \frac{d',h' - d'}{3H} \right) = 149 \left( \frac{1.93 - 0.295}{3} \right) = 45$$

$$\phi_A = \frac{n_A \left( \frac{M_{PMMA}}{\rho_{PEG,PMMA}} \right)}{n_A \left( \frac{M_{PMMA}}{\rho_{PMMA}} \right) + (n_x - 1) \left( \frac{M_{PDMS}}{\rho_{PDMS}} \right)} = \frac{45 \left( \frac{\frac{100g}{mol}}{1.15 \frac{g}{mL}} \right)}{45 \left( \frac{\frac{100g}{mol}}{1.15 \frac{g}{mL}} \right) + (149 - 1) \left( \frac{\frac{1000g}{mol}}{0.96 \frac{g}{mL}} \right)} = 0.043$$

**Fig. S11.** $^1$H-NMR of purified poly[nBA-*ran*-MMA-*g*-(PDMS/PMMA)] brush copolymer series $n_{bb}$=1923, $n_g$=4 synthesized by CRP (400 MHz, CDCl$_3$): 3.89 ((C=O)-O-C**H$_2$**-, PDMS brush, m, 2H), 3.62 ((C=O)-O-C**H$_3$**- and -O-C**H$_2$**-C**H$_2$**-, PMMA and PEG respectively, m, 7H), 0.09 (-(Si(C**H$_3$**)$_2$-O)$_n$-, PDMS macromonomer and brush mixture, s, 68.4H).

**Fig. S12.** $^1$H-NMR of purified poly[nBA-*ran*-MMA-*g*-(PDMS/PMMA)] brush copolymer series $n_{bb}$=1959, $n_g$=8 synthesized by CRP (400 MHz, CDCl₃): 3.89 ((C=O)-O-C**H₂**-, PDMS brush, m, 2H), 3.62 ((C=O)-O-C**H₃**- and -O-C**H₂**-C**H₂**-, PMMA and PEG respectively, m, 7H), 0.09 (-(Si(C**H₃**)₂-O)ₙ-, PDMS macromonomer and brush mixture, s, 68.4H).

Ex. calculation for comb-like grafted A-g-B networks. Sample 100920_5:

$$n_A = n_x \left( \frac{d',h' - d'}{3H} \right) = 139 \left( \frac{5.33 - 0.905}{3} \right) = 205$$

$$\phi_A = \frac{n_A(\frac{M_{PMMA}}{\rho_{PMMA}})}{n_A\left(\frac{M_{PMMA}}{\rho_{PMMA}}\right)+\left(\frac{n_x}{n_g}\right)\left(\frac{M_{PDMS}}{\rho_{PDMS}}\right)+(n_x-\frac{n_x}{n_g})(\frac{M_{PBA}}{\rho_{PBA}})} = \frac{105 \left(\frac{\frac{100g}{mol}}{1.15\frac{g}{mL}}\right)}{105\left(\frac{\left(\frac{100g}{mol}\right)}{\left(1.15\frac{g}{mL}\right)}\right)+\left(\frac{139}{4}\right)\left(\frac{\frac{1000g}{mol}}{0.96\frac{g}{mL}}\right)+(139-\frac{139}{4})\left(\frac{\frac{128g}{mol}}{1.08\frac{g}{mL}}\right)} = 0.268$$
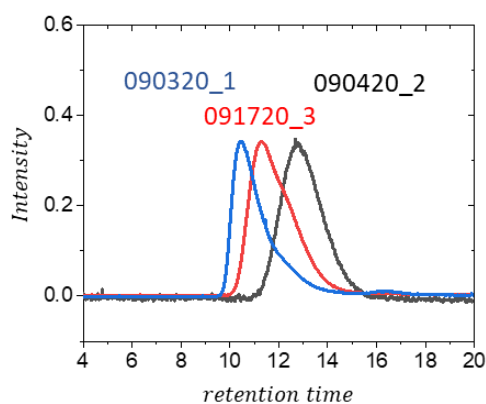
**Fig. S13.** Different $n_{bb}$ verification by gel permeation chromatography for poly[MMA-*g*-(PDMS/PMMA)].
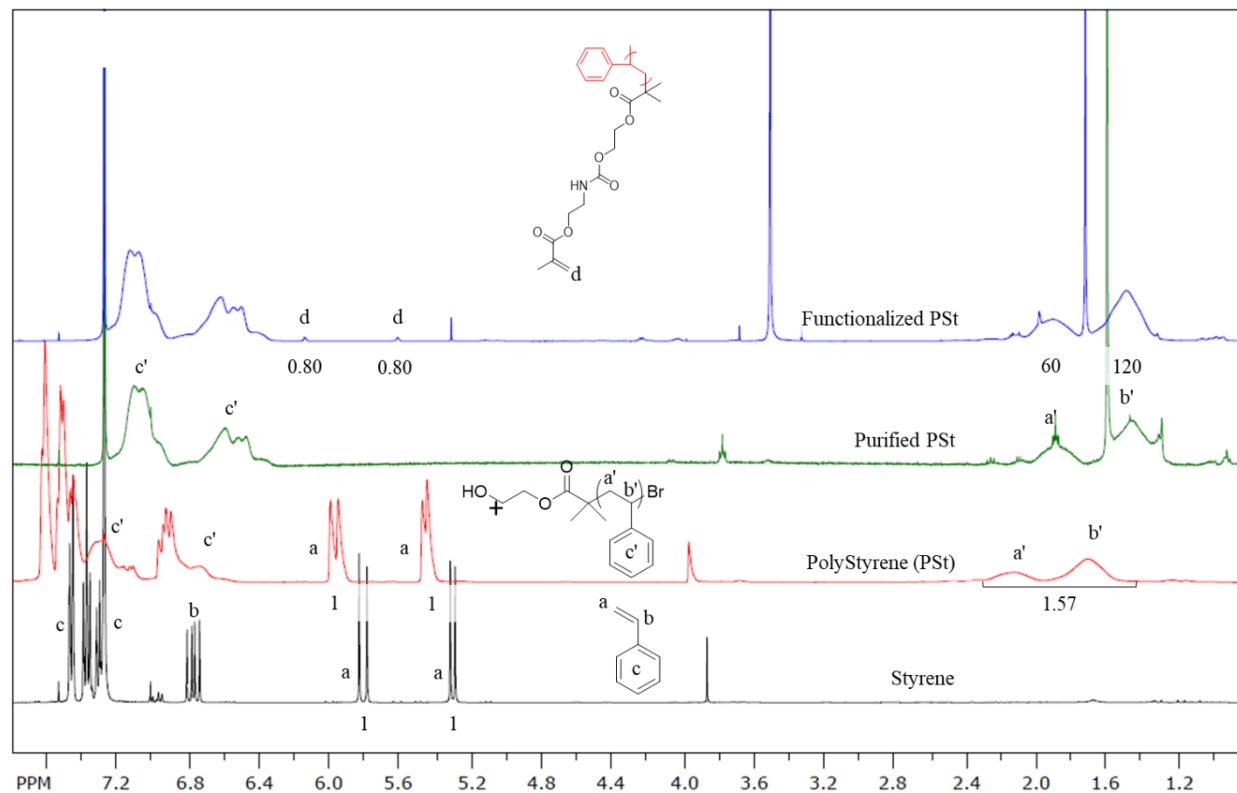


**Fig. S14.** ¹H-NMR of functionalized polystyrene (PS) macromonomers used in FR polymerization at different stages (400 MHz, CDCl₃): 7.66-6.31 ($C_6\mathbf{H_6}$-, residual styrene and PS, m, 6H), 6.15, 5.61 ($\mathbf{CH_2}$=C(CH₃)-C-, functionalized PS, s, 1H), 5.70, 5.46 ($\mathbf{CH_2}$=CH-, residual styrene, s, 1H), 2.16-1.27 (-$\mathbf{CH_2}$-$\mathbf{CH}$-, PS, m, 3H). 3.50, 1.71 (residual methanol), 1.58 (residual water). $n_A$ = [styrene]/[I]*(a'+b')/3/[a/1+ a'+b')/3] = 175 * 1.57/3/[1+1.57/3] = 175*0.34 = 60.1.
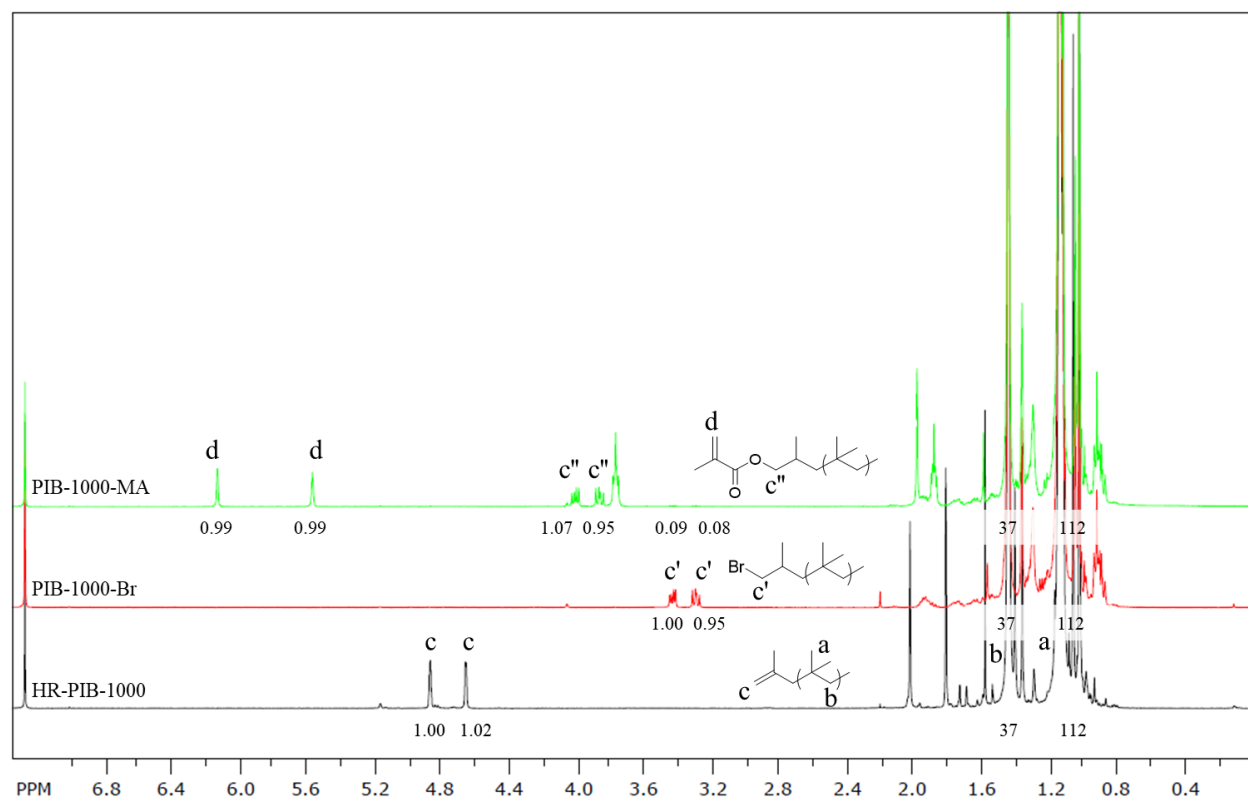
**Fig. S15.** ^{1}H-NMR of PIB macromonomer synthesis (400 MHz, CDCl$_3$): 6.14, 5.58 (**CH$_2$**-C(CH$_3$)-C-, PIB-1000-MA (PIB macromonomer), s, 1H), 4.89, 4.67 (**CH$_2$**=C(CH$_3$)-, HR-PIB-1000, s, 1H), 4.00, 3.87 (-(C=O)-O-C**H$_2$**-, PIB-1000-MA, s, 1H), 3.43, 3.29 (Br-C**H$_2$**-C(CH$_3$)-, PIB-1000-Br, s, 1H), 1.47 (**CH$_2$**-C(CH$_3$)$_2$-, PIB polymer, m, 37H), 1.16 (-CH$_2$-**C(CH$_3$)$_2$**-, PIB polymer, m, 112H).
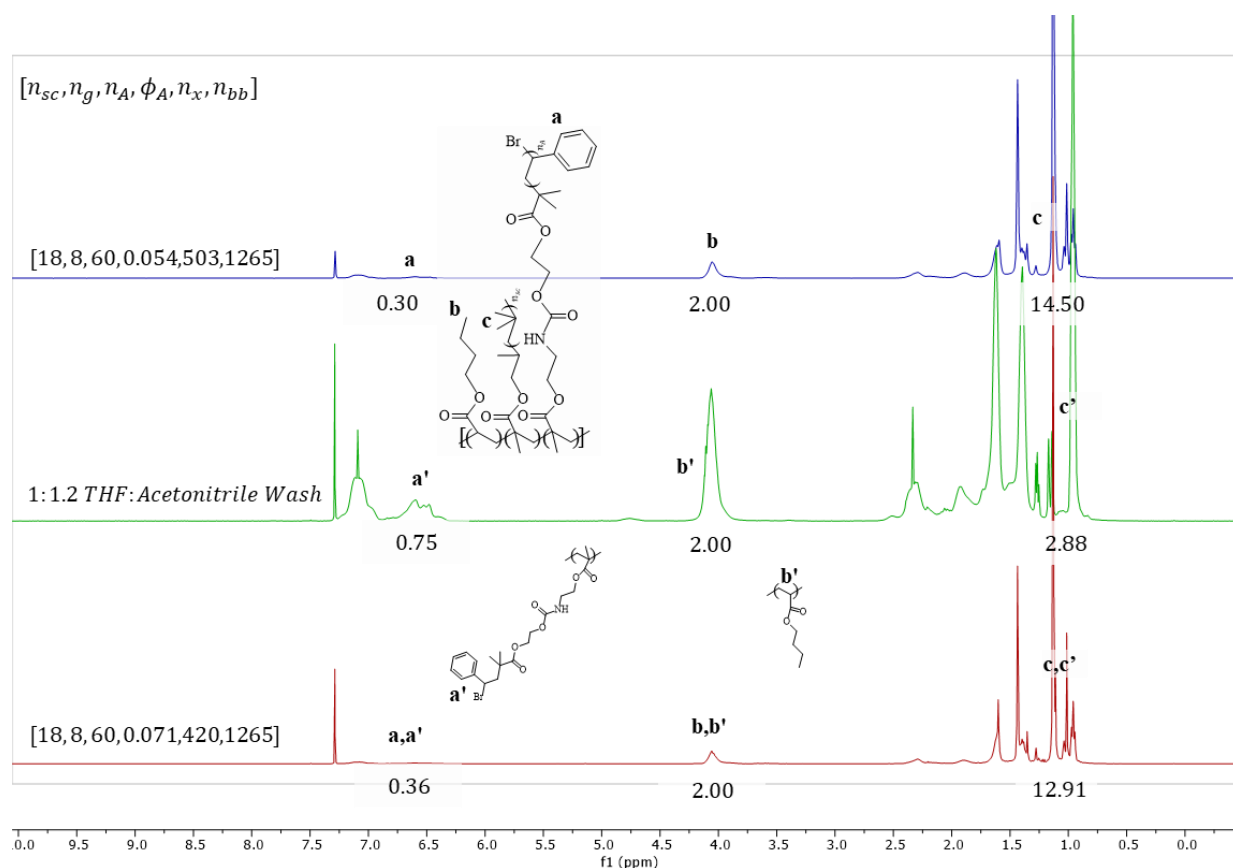
**Fig. S16.** Example wash of poly[nBA-*ran*-MMA-*g*-(PIB/PS)]. From bottom to top: unwashed network, wash supernatant, pure network. Bottom: (400 MHz, CDCl$_3$): 6.56 (CH-CH=C**H**-C-, PS side-chain and unreacted PS oligomer, d, 120H), 4.10 ((C=O)-O-C**H$_2$**-, PBA spacer and unreacted homopolymer, t, 2H), 1.15 (CH$_2$-C-(C**H$_3$)$_2$**-, PIB side chain and unreacted homopolymer, s, 112H). Middle: (400 MHz, CDCl$_3$): 6.56 (CH-CH=C**H**-C-, unreacted PS oligomer, d, 120H), 4.10 ((C=O)-O-C**H$_2$**-, unreacted PBA homopolymer, t, 2H), 1.15 (CH$_2$-C-(C**H$_3$)$_2$**-, unreacted PIB homopolymer, s, 112H). Top: (400 MHz, CDCl$_3$): 6.56 (CH-CH=C**H**-C-, PS side-chain, d, 120H), 4.10 ((C=O)-O-C**H$_2$**-, PBA spacer, t, 2H), 1.15 (CH$_2$-C-(C**H$_3$)$_2$**-, PIB side chain, s, 112H).
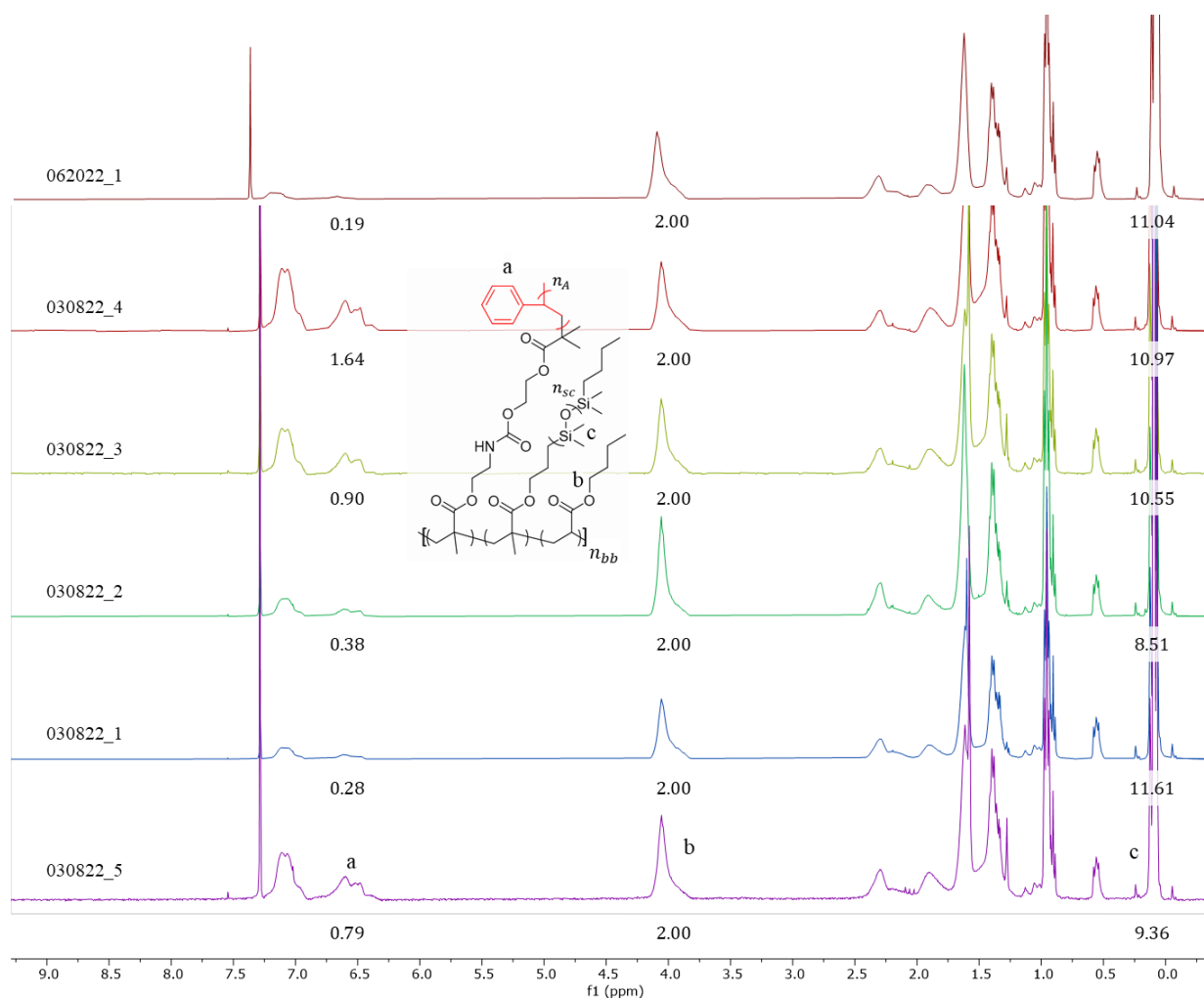
**Fig. S17.** $^{1}$H-NMR of purified poly[nBA-*ran*-MMA-*g*-(PDMS/PS)]. (400 MHz, CDCl$_3$): 6.56 (CH-CH=C**H**-C-, PS side-chain, d, 120H), 4.07 ((C=O)-O-C**H$_2$**-, PBA spacer, d, 2H), 0.09 (-(Si(C**H$_3$**)$_2$-O)$_n$-, PDMS macromonomer and brush mixture, s, 68.4H).



| Sample | $M_n$ (kg/mol) | Đ |
|---|---|---|
| 062022_1 | 231 | 1.74 |
| 030822_1 | 283 | 2.24 |
| 030822_2 | 899 | 2.42 |
| 030822_3 | 808 | 2.14 |
| 030822_4 | 1407 | 2.41 |
| 030822_5 | 1497 | 2.09 |
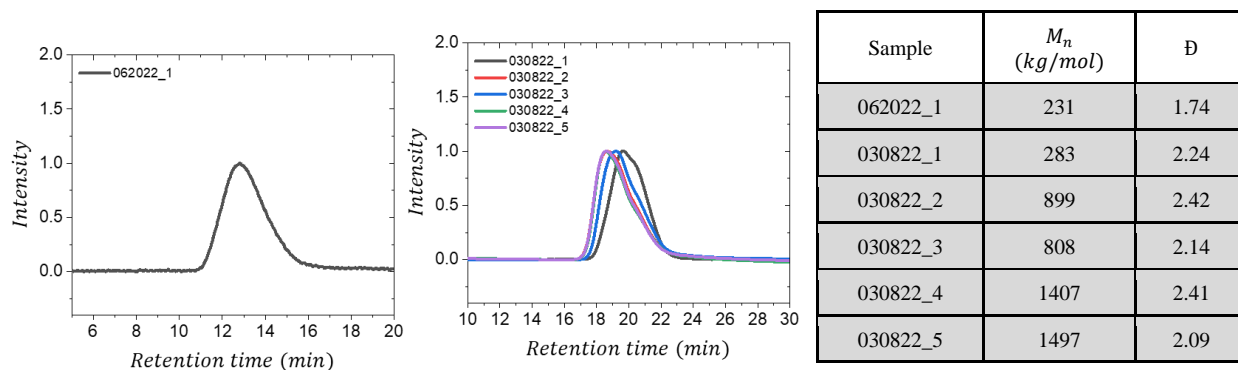
**Fig. S18**. GPC of poly[nBA-*ran*-MMA-*g*-(PDMS/PS)]. 1mg/mL, HALS. Note: sample 062022_1 was run on a 30-minute run cycle while the others were run on a 60-minute run cycle.

Ex. calculation:

$$n_x = \frac{2H * n_A}{a} + [(\frac{2H * n_A}{a})/(\frac{112H}{c})] + 1 = \frac{2*60}{0.90} + [(\frac{2*60}{0.90})/(\frac{68.4}{10.55})] + 1 = 155$$

$$z = \frac{M_n}{M_{n\,PBA}(\frac{2H*n_A}{a}) + M_{n\,PDMS}[(\frac{2H*n_A}{a})/(\frac{68.4H}{c})] + M_{n\,PS}(1)} = \frac{808000 \; g/mol}{128(\frac{2*60}{0.90}) + 1000[(\frac{2*60}{0.90})/(\frac{68.4}{10.55})] + 6240(1)} = 18.4$$

$$n_{bb} = n_x * z = 155 * 18.4 = 2854$$

$$\phi_A = \frac{(\frac{M_{n,PS}}{\rho_{PS}})}{\frac{M_{PBA}}{\rho_{PBA}}(\frac{2H*n_A}{a}) + \frac{M_{n,PDMS}}{\rho_{PDMS}}[(\frac{2H*n_A}{a})/(\frac{68.4H}{c})] + \frac{M_{n,PS}}{\rho_{PS}}} = \frac{\left(\frac{\frac{6240g}{mol}}{1.02\frac{g}{mL}}\right)}{\left(\frac{\frac{128g}{mol}}{1.08\frac{g}{mL}}\right)(\frac{2*60}{0.90}) + \left(\frac{\frac{1000g}{mol}}{0.96\frac{g}{mL}}\right)[(\frac{2*60}{0.90})/(\frac{68.4}{10.55})] + \left(\frac{\frac{6240g}{mol}}{1.02\frac{g}{mL}}\right)} = 0.151$$
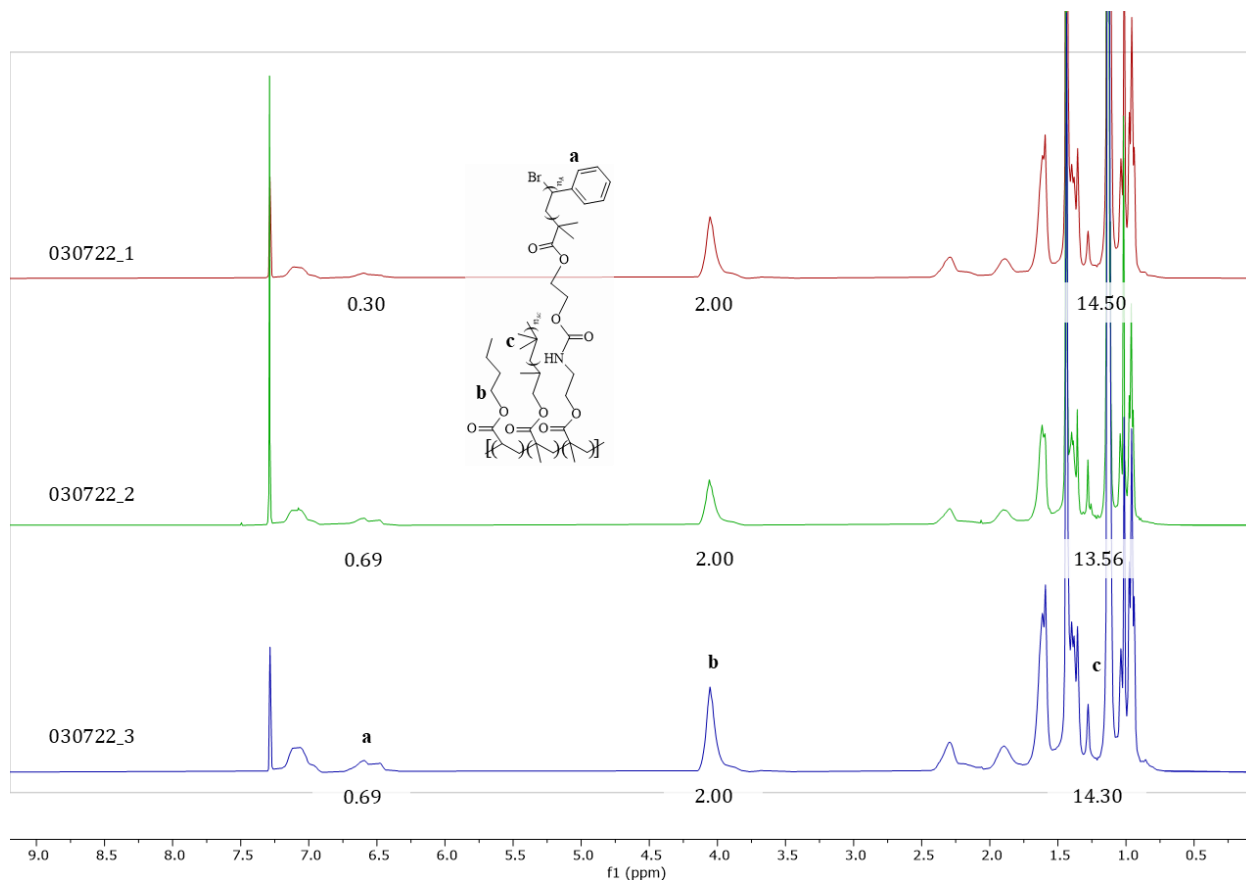


**Fig. S19.** $^1$H-NMR of purified poly[nBA-*ran*-MMA-*g*-(PIB/PS)]. [. (400 MHz, CDCl$_3$): 6.56 (CH-CH=C**H**-C-, PS side chain, d, 120H), 4.10 ((C=O)-O-C**H₂**-, PBA spacer, t, 2H), 1.15 (CH₂-C-(C**H₃)₂**-, PIB side chain, s, 112H).
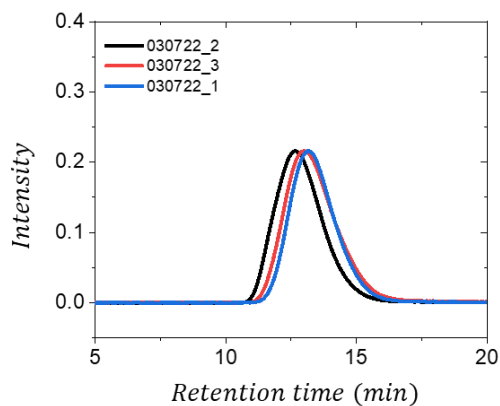
| Sample | $M_n$ $(kg/mol)$ | Đ |
|--------|------------------|---|
| 030722_1 | 204 | 1.70 |
| 030722_2 | 327 | 1.78 |
| 030722_3 | 218 | 1.98 |

**Fig. S20**. GPC of poly[nBA-*ran*-MMA-*g*-(PIB/PS)]. 1mg/mL, HALS. Note: the samples were run on a 30-minute run cycle.

Ex. calculation:

$$n_x = \frac{2H * n_A}{a} + [(\frac{2H * n_A}{a})/(\frac{112H}{c})] + 1 = \frac{2 * 60}{0.69} + [(\frac{2 * 60}{0.69})/(\frac{112}{13.56})] + 1 = 216$$

$$z = \frac{M_n}{M_{n\,PBA}(\frac{2H * n_A}{a}) + M_{n\,PIB}[(\frac{2H * n_A}{a})/(\frac{112H}{c})] + M_{n\,PS}(1)} = \frac{204000}{128(\frac{2 * 60}{0.69}) + 1000[(\frac{2 * 60}{0.69})/(\frac{112}{13.56})] + 6240(1)} = 6.60$$

$$n_{bb} = n_x * z = 216 * 6.60 = 1425$$

$$\phi_A = \frac{(\frac{M_{n,PS}}{V_{PS}})}{\frac{M_{PBA}}{\rho_{PBA}}(\frac{2H * n_A}{a}) + \frac{M_{n,PIB}}{\rho_{PIB}}[(\frac{2H * n_A}{a})/(\frac{112H}{c})] + \frac{M_{n,PS}}{\rho_{PS}}} = \frac{\left(\frac{\frac{6240g}{mol}}{1.02\frac{g}{mL}}\right)}{\left(\frac{\frac{128g}{mol}}{1.08\frac{g}{mL}}\right)(\frac{2 * 60}{0.69}) + \left(\frac{\frac{1000g}{mol}}{0.96\frac{g}{mL}}\right)[(\frac{2 * 60}{0.69})/(\frac{112}{13.56})] + \left(\frac{\frac{6240g}{mol}}{1.02\frac{g}{mL}}\right)} = 0.108$$

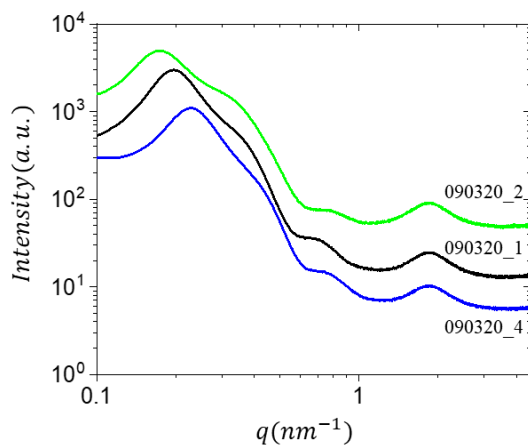## S3. SAXS analysis



**Fig. S21**. SAXS curves of poly[MMA-g-(PDMS/PMMA)] samples with variable $\phi_A$. Analysis reported in main text Table 1.
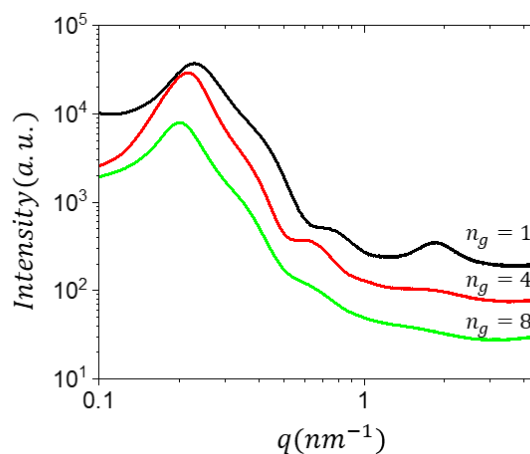


**Fig. S22**. SAXS curves of poly[nBA-ran-MMA-g-(PDMS/PMMA)] samples with variable $n_g$ and $\phi_A$ (cf. Table 1).

## S4. Atomic force microscopy.



700 nm

**Fig. S23**. LB-monolayer of poly[MMA-*g*-(PDMS/PMMA)], sample 090320_4.

## S5. Mechanical Properties

**Table S1**. Structural and mechanical parameters of soft biological tissue.

| Sample | $E^{6)}(MPa)$ | $\beta^{6)}$ | $E_0^{7)}(kPa)$ | $\sigma_{max}{}^{9)}$ $(MPa)$ | Reference |
|---|---|---|---|---|---|
| Human abdominal skin | 1.20 | 0.93 | 164 | 13 | [11] |
| Porcine brain tissue | 1.00 | 0.72 | 8.90 | 2.4 | [12] |
| Artery adventitia A | 0.35 | 0.91 | 28.8 | 2.5 | [13] |
| Pig belly | 5.46 | 0.45 | 13.8 | 1.2 | [14] |
| Porcine aorta | 19.8 | 0.67 | 128 | 2.0 | [15,16] |
| Bovine nuchal ligament | 0.15 | 0.93 | 20.0 | 5.0 | [1,16*] |
| Vena cava | 3.40 | 0.75 | 37.4 | 4.5 | [1,17*] |
| Carotid artery | 0.35 | 0.91 | 28.8 | 2.8 | [1,17*] |
| Skeletal muscle tissue | 2.02 | 0.54 | 7.00 | 2.8 | [1,18*] |
| Human aorta: superior | 21.0 | 0.72 | 185 | 6.7 | [19] |
| Human aorta: high | 105 | 0.55 | 380 | 4.6 | [19] |
| Human aorta: Sinotubular junction | 50.1 | 0.45 | 381 | 7.1 | [20] |
| Ligament | Frequency Sweep from Fig. 4d | | | | [21] |

| Bovine Paracardium | Frequency Sweep from Fig. 4d | 22 |
|---|---|---|
| Porcine Brain | Frequency Sweep from Fig. 4d | 23 |

*$E$, $\beta$, and $E_0$ values correspond to class of tissue from ref. 1.

**Table S2**. Architectural parameters and mechanical properties of A-g-B brush copolymers.

| Sample | $n_g$ [1] | $n_{sc}$ | $n_x$ [2] | $n_A$ [3] | $\phi_A$ [4] | $n_{bb}$ [5] | $E$ [6] $(kPa)$ | $\beta$ [6] | $E_0$ [7] $(kPa)$ | $\lambda_{fit}$ [8] | $\lambda_{max}$ [9] | $\sigma_{max}$ [10] $(kPa)$ |
|---|---|---|---|---|---|---|---|---|---|---|---|---|
| poly[MMA-*g*-(PDMS/PMMA)] | | | | | | | | | | | | |
| 090320_2 | 1 | 14 | 149 | 27 | 0.015 | 1935 | 5.65 | 0.31 | 9.8 | 2.10 | 2.81 | 104 |
| 090320_1 | 1 | 14 | 149 | 62 | 0.034 | 1935 | 14.4 | 0.40 | 31.4 | 1.90 | 2.92 | 605 |
| 090320_4 | 1 | 14 | 149 | 81 | 0.044 | 1935 | 20.5 | 0.46 | 53.1 | 1.70 | 2.98 | 898 |
| 091720_2 | 1 | 14 | 149 | 46 | 0.025 | 607 | 12.2 | 0.26 | 18.9 | 1.57 | 2.34 | 51.2 |
| 091720_3 | 1 | 14 | 149 | 63 | 0.034 | 607 | 10.5 | 0.45 | 26.6 | 1.65 | 2.07 | 94.3 |
| 111620_2 | 1 | 14 | 149 | 82 | 0.044 | 607 | 14.2 | 0.52 | 45.8 | 1.44 | 1.87 | 122 |
| 111620_1 | 1 | 14 | 149 | 148 | 0.077 | 607 | 15.1 | 0.52 | 48.6 | 1.64 | 1.84 | 144 |
| 090420_3 | 1 | 14 | 149 | 53 | 0.029 | 210 | 7.30 | 0.42 | 16.9 | 1.80 | 2.04 | - |
| 090420_2 | 1 | 14 | 149 | 66 | 0.036 | 210 | 4.38 | 0.51 | 13.6 | 1.45 | 1.52 | 10.6 |
| 090420_1 | 1 | 14 | 149 | 99 | 0.053 | 210 | 11.7 | 0.54 | 40.7 | 1.28 | 1.69 | 36.8 |
| 090420_4 | 1 | 14 | 149 | 152 | 0.079 | 210 | 13.6 | 0.57 | 53.5 | 1.54 | 1.63 | 84.4 |
| poly[nBA-*ran*-MMA-*g*-(PDMS/PMMA)] | | | | | | | | | | | | |
| 100920_2 | 4 | 14 | 139 | 85 | 0.131 | 1923 | 36.3 | 0.18 | 47.9 | 2.50 | 3.40 | 606 |
| 100920_1 | 4 | 14 | 139 | 178 | 0.241 | 1923 | 61.6 | 0.29 | 103 | 2.20 | 2.83 | 1223 |
| 100920_5 | 4 | 14 | 139 | 205 | 0.268 | 1923 | 77.3 | 0.33 | 142 | 1.96 | 2.96 | 2572 |
| 100820_3 | 8 | 14 | 142 | 48 | 0.112 | 1959 | 15.8 | 0.09 | 18.0 | 3.32 | 4.95 | 558 |
| 100820_2 | 8 | 14 | 142 | 147 | 0.278 | 1959 | 50.4 | 0.13 | 60.9 | 3.25 | 5.21 | 2653 |
| 100820_1 | 8 | 14 | 142 | 187 | 0.329 | 1959 | 68.6 | 0.15 | 86.1 | 3.00 | 4.62 | 2674 |
| poly[nBA-*ran*-MMA-*g*-(PDMS/PS)] | | | | | | | | | | | | |
| 062022_1* | 8 | 14 | 844 | 60 | 0.03 | 1021 | 11.4 | 0.08 | 18.5 | 2.91 | 3.46 | 81.0 |
| 030822_1** | 8 | 14 | 502 | 60 | 0.05 | 1061 | 47.4 | 0.18 | 78.1 | 2.37 | 2.78 | 256 |
| 030822_2 | 8 | 14 | 315 | 60 | 0.08 | 2807 | 77.1 | 0.22 | 110 | 2.13 | 2.71 | 610 |
| 030822_3 | 8 | 14 | 155 | 60 | 0.15 | 2854 | 209 | 0.44 | 528 | 1.64 | 2.23 | 2588 |
| 030822_4 | 8 | 14 | 86 | 60 | 0.24 | 4425 | 210 | 0.72 | 1853 | 1.24 | 2.09 | 5430 |

| | | | | | | | | | | | | |
|---|---|---|---|---|---|---|---|---|---|---|---|---|
| 030822_5 | 10 | 14 | 178 | 60 | 0.15 | 5573 | 286 | 0.50 | 858 | 1.52 | 2.57 | 6000 |
| poly[nBA-*ran*-MMA-*g*-(PIB/PS)] | | | | | | | | | | | | |
| 030722_1 | 8 | 18 | 503 | 60 | 0.048 | 940 | 46.8 | 0.16 | 59.9 | 2.49 | 3.85 | 740 |
| 030722_2 | 8 | 18 | 216 | 60 | 0.108 | 1425 | 170 | 0.20 | 232 | 2.32 | 4.67 | 3520 |
| 030722_3 | 8 | 18 | 218 | 60 | 0.106 | 938 | 133 | 0.23 | 193 | 2.35 | 3.46 | 2040 |

[1] Grafting density of side chains on the backbone with BA spacer. [2] Number average degree polymerization of brush backbone between glassy block side chains that physical crosslink. [3] Number average degree polymerization of each glassy block side chain as determined by $^1$H-NMR. [4] Volume fraction glassy block, $\rho_{PMMA} = 1.15\,g/mL$, $\rho_{PIB} = 0.92\,g/mL$, $\rho_{PS} = 1.02\,g/mL$, $\rho_{PDMS} = 0.96\,g/mL$, $\rho_{PEG} = 0.94\,g/mL$, $\rho_{PBA} = 1.08\,g/mL$. [5] Number average degree polymerization of the total brush strand. [6] Structural modulus $E \sim 1/\big(n_{bb}(n_{sc} + 1)\big)$ and strain-stiffening parameter $\beta = \langle R_{in}^2 \rangle / R_{max}^2$ are fitting parameters in equation S1. [7] Apparent Young's modulus which can be determined either as tangent of a stress-strain curve at $\lambda \rightarrow 1$ or from the fitting equation S2. [8] Elongation range used for fitting equation S1 before deviation from the theory. [9] Maximum true stress and elongation at sample rupture. [10] Maximum stress-at-break (strength) of A-g-B brush copolymer samples. $*G_e = 1.9\,kPa$. $**G_e = 5.1\,kPa$.
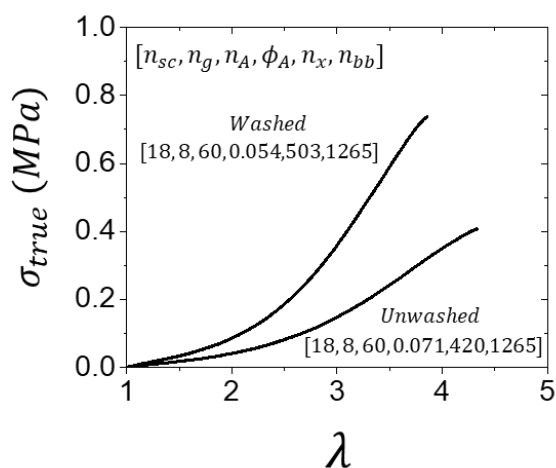


**Fig. S24. Example** Stress-elongation dependence on removing unreacted reagent, poly[nBA-*ran*-MMA-*g*-(PIB/PS)]. $\dot{\varepsilon}$ =0.001, T=22°C.
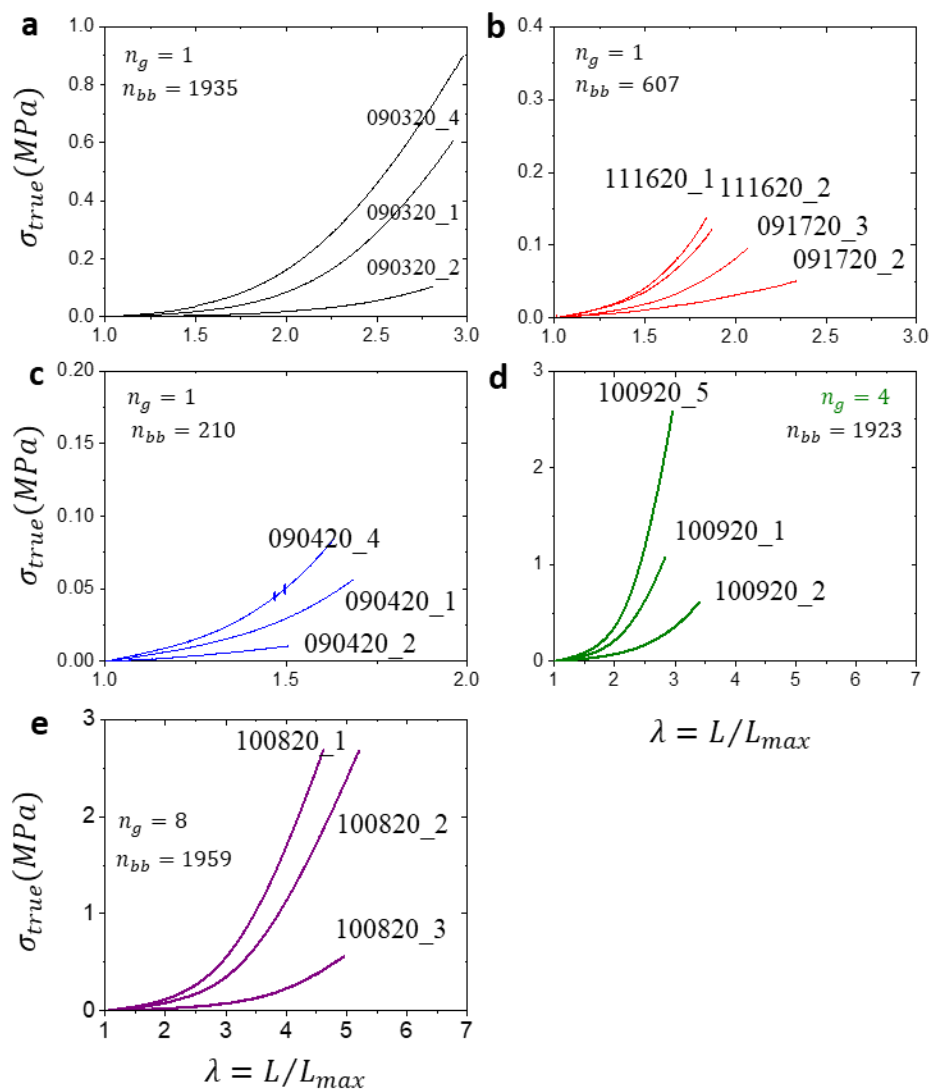
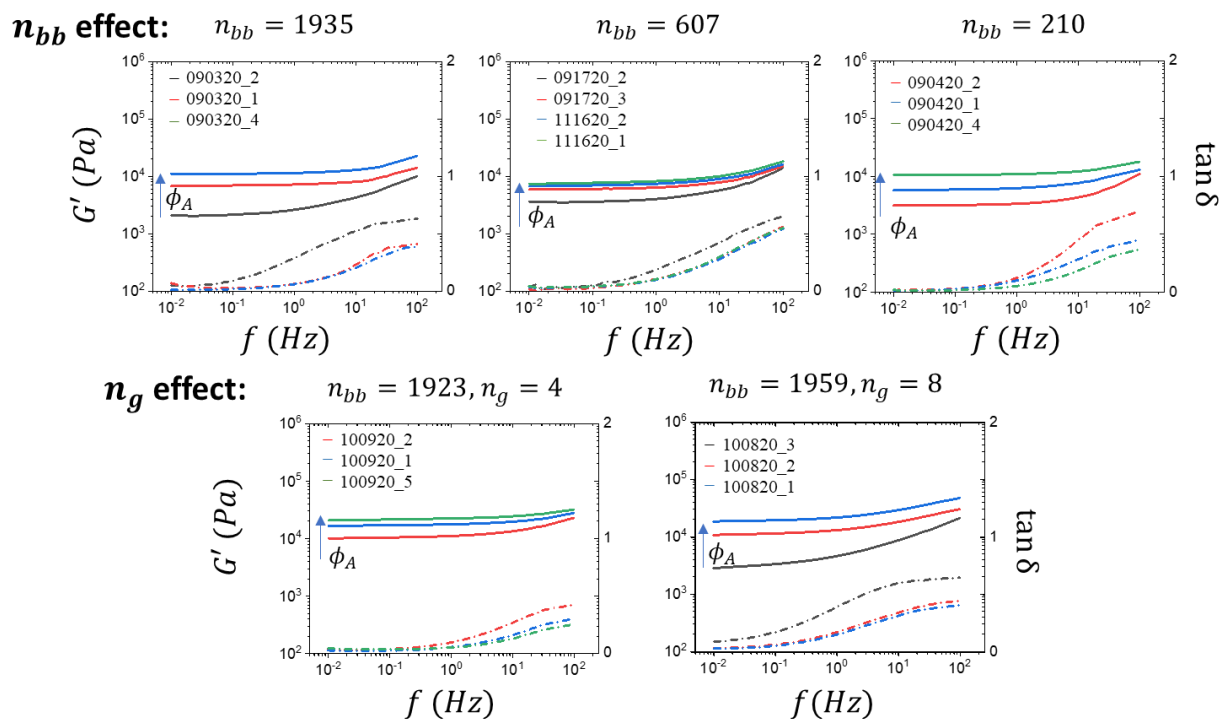**Fig. S25**. True stress-elongation curve profiles of poly[MMA-*g*-(PDMS/PMMA)] and poly[nBA-*ran*-MMA-*g*-(PDMS/PMMA)] b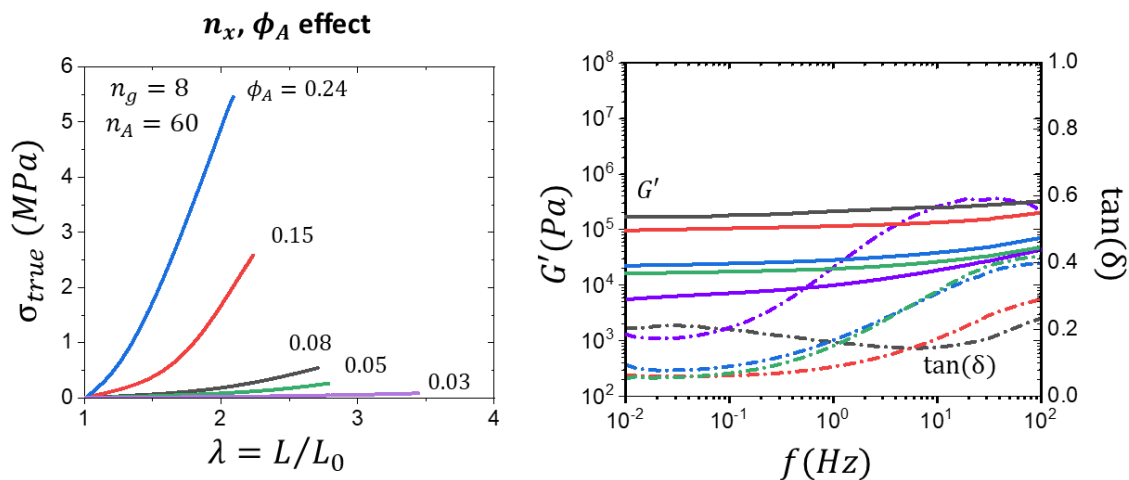rush graft copolymers synthesized by CRP. a) Series $n_{bb}$ = 1935, $n_g$ = 1. b) Series $n_{bb}$ = 607, $n_g$ = 1. c) Series $n_{bb}$ = 210, $n_g$ = 1. d) Series $n_{bb}$ = 1923, $n_g$ = 4. e) Series $n_{bb}$ = 1959, $n_g$ = 8. $\dot{\varepsilon}$ =0.005, T=22°C.

**Fig. S26**. Oscillatory frequency sweeps of poly[MMA-*g*-(PDMS/PMMA)] and poly[nBA-*ran*-MMA-*g*-(PDMS/PMMA)] brush graft copolymers synthesized by CRP. ε=0.05, T=22°C.



**Fig. S27.** Stress-elongation ($\dot{\varepsilon}$ =0.005) and oscillatory frequency sweeps of poly[nBA-*ran*-MMA-*g*-(PDMS/PS)]. ε=0.05, T=22°C.
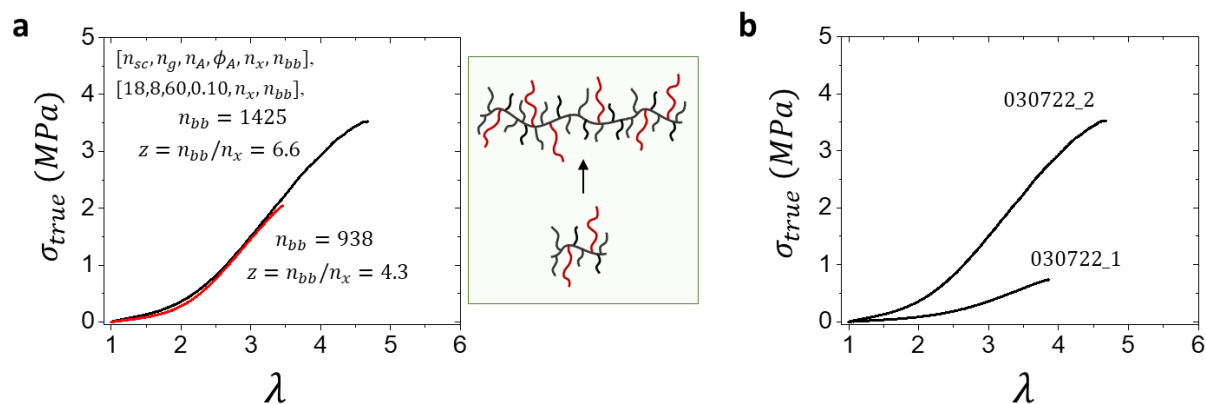
**Fig. S28.** Stress-elongation of poly[nBA-*ran*-MMA-*g*-(PIB/PS)]. a) $n_{bb}$ effect on poly[nBA-*ran*-MMA-*g*-(PIB/PS)] through FR polymerization. Initiator concentration was varied to change $n_{bb}$. b) Changing $\phi_A$ and $n_x$ control mechanical properties. $\dot{\varepsilon}$ =0.001, T=22°C.
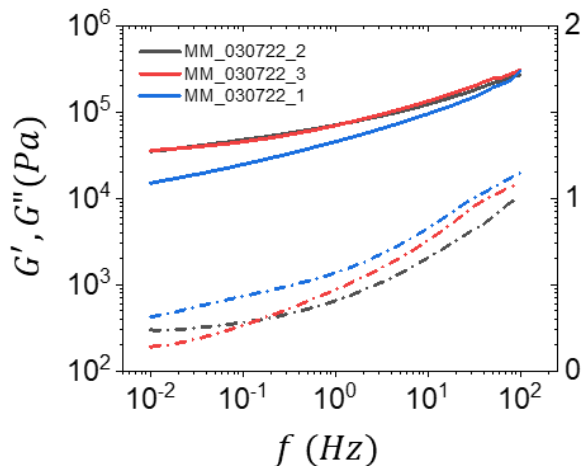


**Fig. S29.** Oscillatory frequency sweeps of poly[nBA-*ran*-MMA-*g*-(PIB/PS)]. $\varepsilon$=0.05, T=22°C.
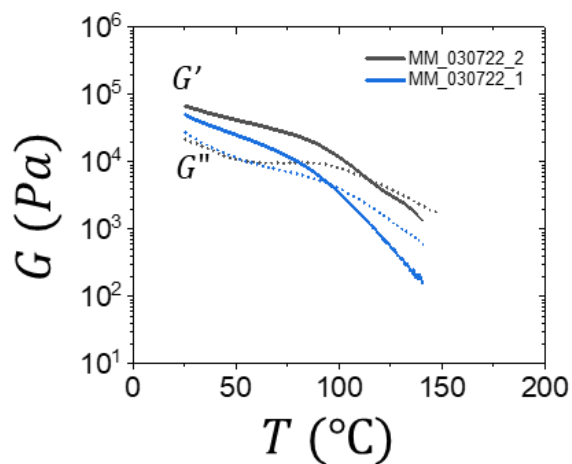


**Fig. S30.** Temperature evolution of poly[nBA-*ran*-MMA-*g*-(PIB/PS)]. $\varepsilon$=0.05, $f = 1\ Hz$.
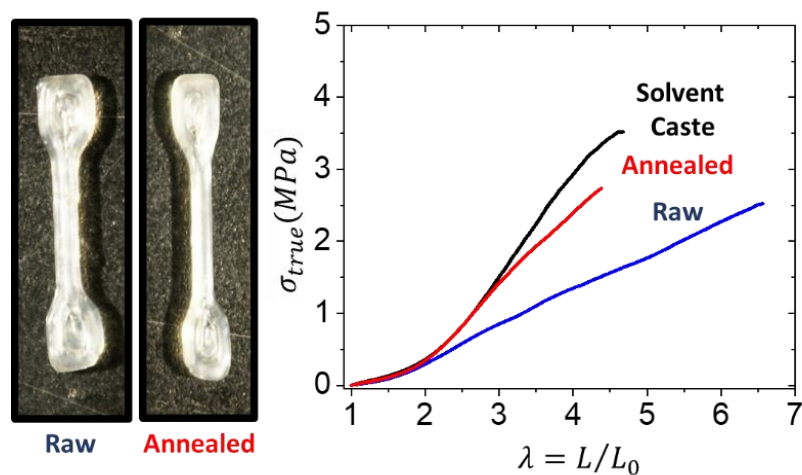
**Fig. S31.** 3D printed dog bones experience identical stress-elongation response after annealing to solvent caste preparation. Sample 030722_2. $\dot{\varepsilon}$ =0.001, T=22°C.
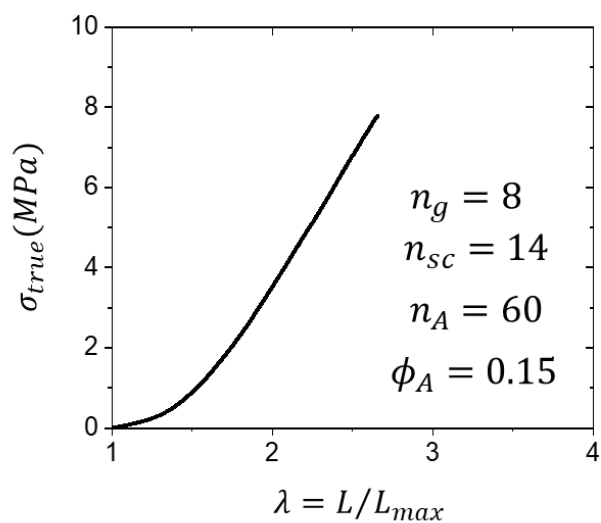


**Fig. S32.** PS-g-PDMS ($n_g$=8) series with additional covalent crosslinking. A-g-B polymers can be covalently crosslinked in addition to physical crosslinks. This was achieved by formulating PS-g-PDMS ($n_g$=8) and curing under nitrogen in a mold for an extended period of time (>72hr).

## S6. Computer simulation of A-g-B graft copolymer networks

We have performed coarse-grained molecular dynamics simulations of self-assembled graft copolymers consisting of semiflexible thick backbone and grated flexible side chains (Fig. S33). Each side chain with $n_A = 5$ monomers was separated by backbone block of $n_x = 20$ monomers. The copolymer chains were modelled as bead-spring chains with different bead sizes. This was done by implementing the modified, truncated, shifted Lennard-Jones (LJ) potential with an offset to the interaction range by $\Delta$.
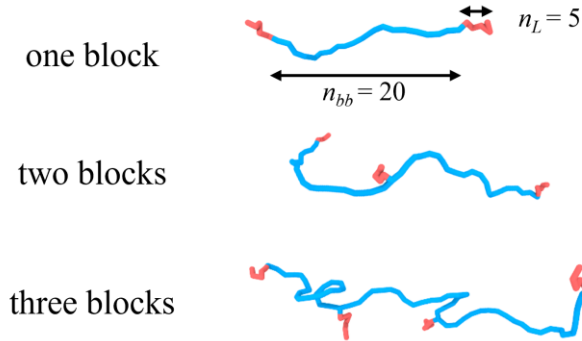


**Fig. S33.** Snapshots of block copolymers made by grafting flexible chains with $n_A$ monomers (shown in red) to semiflexible backbone (shown in blue).

$$U_{\text{LJ}}(r) = \begin{cases} 4\varepsilon_{\text{LJ}}\left[\left(\frac{\sigma}{r-\Delta}\right)^{12} - \left(\frac{\sigma}{r-\Delta}\right)^{6} - \left(\frac{\sigma}{r_{\text{cut}}}\right)^{12} + \left(\frac{\sigma}{r_{\text{cut}}}\right)^{6}\right] & r \leq r_{\text{cut}} + \Delta \\ 0 & r > r_{\text{cut}} + \Delta \end{cases} \tag{S4}$$

The connectivity of beads into chains was represented by the sum of the finite extensible nonlinear elastic (FENE) potential

$$U_{\text{FENE}}(r) = -0.5k_{\,spring}R_{\max}^2 \ln(1 - (r - \Delta)^2/R_{\max}^2) \tag{S5}$$

with spring constant $k_{spring} = 30\ k_B T/\sigma^2$ and the maximum bond length $R_{max} = 1.5\sigma$ and the pure repulsive modelled by the modified truncated-shifted LJ potential with $\varepsilon_{\text{LJ}} = 1.0 k_B T$ and $r_{\text{cut}} = 2^{1/6}\sigma$ for backbone-backbone(B-B) pairs and linear-backbone (L-B) pair and $\varepsilon_{\text{LJ}} = 0.8 k_B T$ and $r_{\text{cut}} = 2^{1/6}\sigma$ for linear-linear (L-L) pairs. In our simulation, the value of the parameter $\Delta = 0$ for the B-B pairs, $\Delta = -0.5\sigma$ for the L-L pairs, and $\Delta = -0.25\sigma$ for the L-B pairs. Based on these settings, the diameters of the identical backbone and linear side chain beads were equal to $1.0\sigma$ and $0.5\sigma$, respectively.

The bending rigidity of the backbone was introduced by imposing the bending potential controlling mutual orientations between two neighboring along the backbone unit bond vectors $\boldsymbol{n}_i$ and $\boldsymbol{n}_{i+1}$.

$$U_{i,i+1}^{bend} = k_{\mathrm{B}}TK\big(1 - (\boldsymbol{n}_i \cdot \boldsymbol{n}_{i+1})\big) \tag{S6}$$

where $K = 5.0$ and $k_{\mathrm{B}}T$ is the thermal energy set to 1.0 in the energy units.

Simulations of copolymer systems were carried out in a constant volume with 3-D periodic boundary conditions at a constant temperature ensemble. The constant temperature was maintained by coupling the system to a Langevin thermostat implemented in LAMMPS.[4] In this representation, the equation of motion of the $i$-th bead is given by

$$m\frac{d\boldsymbol{v}_i(t)}{dt} = \boldsymbol{F}_i(t) - \xi\boldsymbol{v}_i(t) + \boldsymbol{F}_i^R(t) \tag{S7}$$

where $m$ is the bead mass set to unity for all beads, $\boldsymbol{v}_i(t)$ is the $i$th bead velocity, $\boldsymbol{F}_i(t)$ is the net deterministic force acting on the $i$th bead, and $\boldsymbol{F}_i^R(t)$ is the stochastic force with a zero average and a δ-function correlation $\big\langle \boldsymbol{F}_i^R(t) \cdot \boldsymbol{F}_j^R(t') \big\rangle = 6k_BT\xi\delta_{ij}\delta(t - t')$. The friction coefficient was set to $\xi = 0.1m/\tau_{LJ}$, where $\tau_{LJ} = \sigma(m/k_BT)^{1/2}$ is the standard LJ-time. The velocity-Verlet algorithm with a time step $\Delta t = 0.005\tau_{LJ}$ was used for the integration of the equation of motion. All simulations were performed using LAMMPS.[24]

**Table S3** Number of beads in studied systems

| total number of beads | 1 block | 2 blocks | 3 blocks |
|---|---|---|---|
| linear side chains | 33200 | 27465 | 25280 |
| backbones | 73040 | 78733 | 80896 |

Systems were prepared by first randomly placing copolymer chains with number of beads summarized in **Table S3** in a cubic $50\sigma \times 50\sigma \times 50\sigma$ simulation box with a monomer density $\rho = 0.85\sigma^{-3}$. In the beginning, the non-bonded interaction potentials between all beads were set to be the same, with $\varepsilon_{\mathrm{LJ}} = 1.0k_BT$, $r_{cut} = 2^{1/6}\sigma$, and the conformations of chains were relaxed according to the method described in our previous work.[25,26] To trigger the self-assembly, the interaction parameter between monomers belonging to the flexible side chains was gradually changed to an attractive truncated-shifted LJ potential with $r_{cut} = 2.5\sigma$ and $\varepsilon_{\mathrm{LJ}}$ from $0.1k_BT$ to $0.8k_BT$ with an increment of $0.1k_BT$ every $5 \times 10^3\varepsilon_{\mathrm{LJ}}$. Then, a follow-up canonical *NVT* simulation run lasting 5

$\times 10^4 \varepsilon_{\text{LJ}}$ was performed to complete the equilibration of the self-assembled network. For this simulation, the interaction parameters $(\varepsilon_{\text{LJ}}, r_{cut})$ were set to $(1.0 k_B T, 2^{1/6}\sigma)$ for B-B pairs, $(1.0 k_B T, 2^{1/6}\sigma)$ for B-L pairs, and $(0.8 k_B T, 2.5\sigma)$ for L-L pairs.

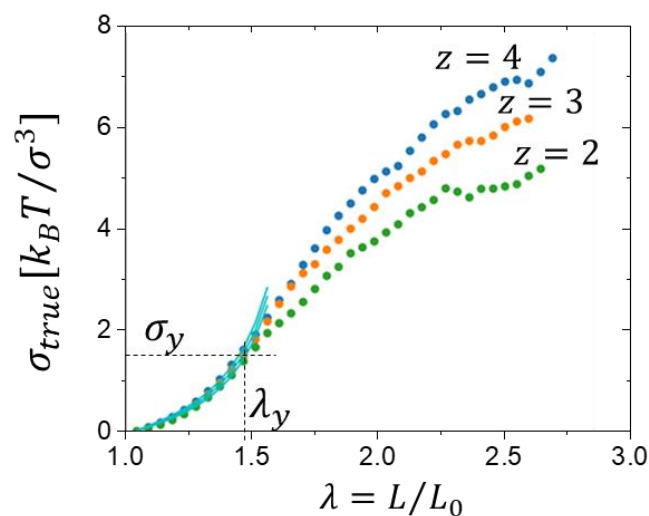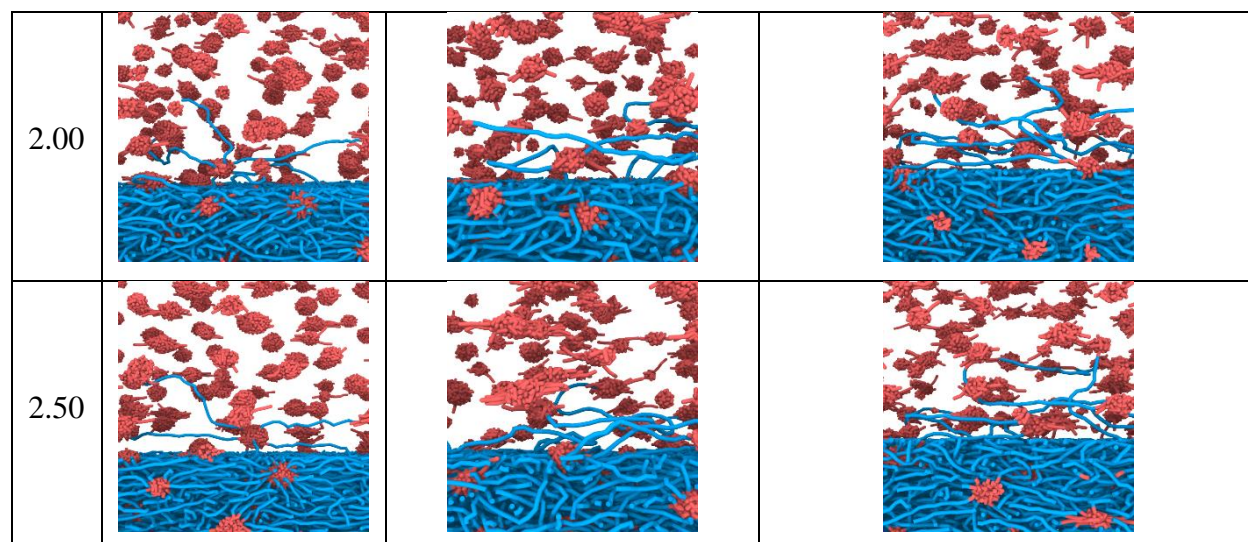**Table S4**. Snapshots of deformation (horizontal plane) of self-assembled networks of graft copolymers

| $\lambda$ | | | |
|---|---|---|---|
| 1.0 | | | |
| 1.25 | | | |
| 1.50 | | | |
| 1.75 | | | |

| | | | |
|---|---|---|---|
| 2.00 | | | |
| 2.50 | | | |
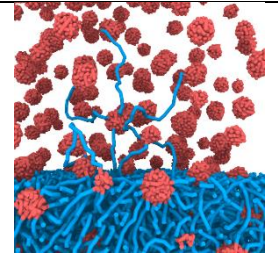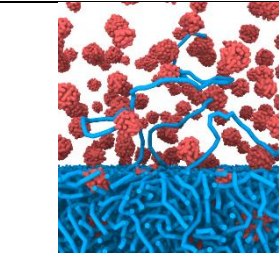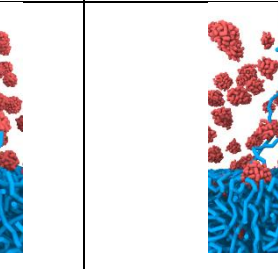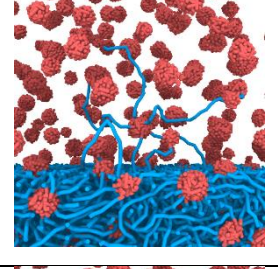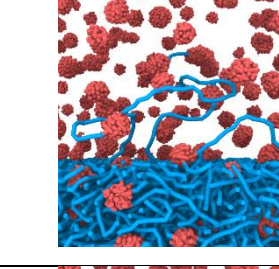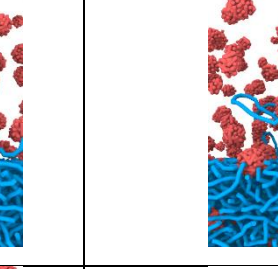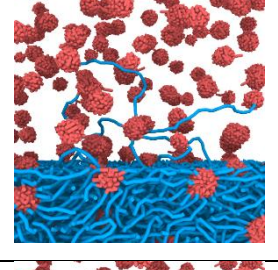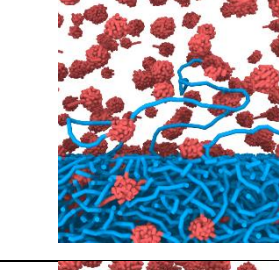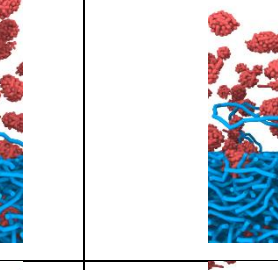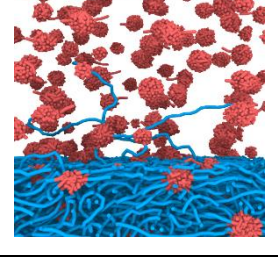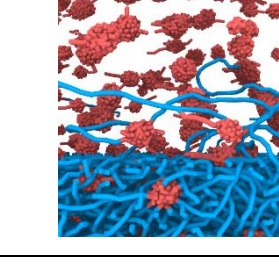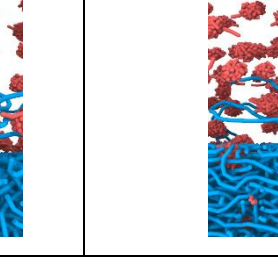


**Fig. S34.** Dependence of the tensile stress $\sigma_{true}$ on the deformation ratio $\lambda$ for self-assembled networks of copolymers consisting of one backbone block (green circles), two blocks (orange circles), and three blocks (blue circles).

To obtain the stress-strain curves shown in Fig. S34, the uniaxial deformation simulations were performed at a constant volume as described in previous work.[27] It follows from this figure that at small deformations and initial stages of the nonlinear deformation regime self-assembled network mechanical properties are almost identical and independent of the number of grafted flexible chains. This points out that in this deformation regime, network mechanical properties are determined by deformation of the backbone blocks connecting network nodes made by self-assembled chains. The departure from universal behavior begins when self-assembled domains

start to deform as illustrated in **Table S4** representing snapshots of networks at different deformation ratios. This first happens for networks of copolymers with the smallest number of backbone blocks. This trend is consistent with experimentally observed behavior in studied bottlebrush systems.

## S7. References

1  A. N. Keith, M. Vatankhah-Varnosfaderani, C. Clair, F. Fahimipour, E. Dashtimoghadam, A. Lallam, M. Sztucki, D. A. Ivanov, H. Liang, A. V. Dobrynin and S. S. Sheiko, *ACS Cent. Sci.*, 2020, **6**, 413–419.

2  Y. Cong, M. Vatankhah-Varnosfaderani, V. Karimkhani, A. N. Keith, F. A. Leibfarth, M. R. Martinez, K. Matyjaszewski and S. S. Sheiko, *Macromolecules*, 2020, **53**, 8324–8332.

3  J.-S. Wang and K. Matyjaszewski, *J. Am. Chem. Soc.*, 1995, **117**, 5614–5615.

4  K. Matyjaszewski, *Macromolecules*, 2012, **45**, 4015–4039.

5  S. R. Kline, *J Appl Cryst*, 2006, **39**, 895–900.

6  A. V. Dobrynin and J.-M. Y. Carrillo, *Macromolecules*, 2011, **44**, 140–146.

7  M. Vatankhah-Varnosfaderani, A. N. Keith, Y. Cong, H. Liang, M. Rosenthal, M. Sztucki, C. Clair, S. Magonov, D. A. Ivanov, A. V. Dobrynin and S. S. Sheiko, *Science*, 2018, **359**, 1509–1513.

8  H. Lakrout, P. Sergot and C. Creton, *Journal Adhes*, 1999, **69**, 307–359.

9  D. J. Walsh, M. A. Wade, S. A. Rogers and D. Guironnet, *Macromolecules*, 2020, **53**, 8610–8620.

10 T. Kelen, F. Tüdös and B. Turcsányi, *Polym Bull*, 1980, **2**, 71–76.

11 F. H. Silver, J. W. Freeman and D. DeVore, *Skin Res Technol*, 2001, **7**, 18–23.

12 B. Rashid, M. Destrade and M. D. Gilchrist, *J Mech Behav Biomed Mater*, 2014, **33**, 43–54.

13 G. A. Holzapfel, G. Sommer, C. T. Gasser and P. Regitnig, *Am J Physiol Heart Circ Physiol*, 2005, **289**, H2048-2058.

14 B. Zhou, F. Xu, C. Q. Chen and T. J. Lu, *Philos Trans R Soc A*, 2010, **368**, 679–690.

15 E. S. Place, J. H. George, C. K. Williams and M. M. Stevens, *Chem. Soc. Rev.*, 2009, **38**, 1139–1151.

16 L. D. Muiznieks and F. W. Keeley, *Biochimica et Biophysica Acta (BBA) - Molecular Basis of Disease*, 2013, **1832**, 866–875.

17 F. H. Silver, P. B. Snowhill and D. J. Foran, *Ann Biomed Eng*, 2003, **31**, 793–803.

18 C. D. Kuthe and R. V. Uddanwadiker, *J Appl Biomater Funct Mater*, 2016, **14**, 154–162.

19 D. Zhalmuratova, T.-G. La, K. T.-T. Yu, A. R. A. Szojka, S. H. J. Andrews, A. B. Adesida, C. Kim, D. S. Nobes, D. H. Freed and H.-J. Chung, *ACS Appl. Mater. Interfaces*, 2019, **11**, 33323–33335.

20 G. S. Carr-White, A. Afoke, E. J. Birks, S. Hughes, A. O'Halloran, S. Glennen, S. Edwards, M. Eastwood and M. H. Yacoub, *Circulation*, 2000, **102**, Iii–15.

21 E. Tanaka, T. Inubushi, J. H. Koolstra, T. M. van Eijden, R. Sano, K. Takahashi, N. Kawai, E. B. Rego and K. Tanne, *Ann Biomed Eng*, 2006, **34**, 1917–1923.

22 H. A. Alhadrami, R. ur R. Syed, A. A. Zahid, R. Ahmed, S. Hasan and A. Hasan, *J Healthc Eng*, 2019, **2019**, e3290370.

23 M. Hrapko, J. a. W. van Dommelen, G. W. M. Peters and J. S. H. M. Wismans, *Biorheology*, 2006, **43**, 623–636.

24 S. Plimpton, *J Comput Phys*, 1995, **117**, 1–19.

25 H. Liang, Z. Cao, Z. Wang, S. S. Sheiko and A. V. Dobrynin, *Macromolecules*, 2017, **50**, 3430–3437.

26 H. Liang, Z. Wang, S. S. Sheiko and A. V. Dobrynin, *Macromolecules*, 2019, **52**, 3942–3950.
27 H. Liang, Z. Wang and A. V. Dobrynin, *Macromolecules*, 2019, **52**, 8617–8624.